Scattering of harmonic P1 and SV waves by a shallow lined circular tunnel in a poroelastic half-plane

Liu, Qijian; Yue, Cheng; Zhao, Mingjuan

Important note
To cite this publication, please use the final published version (if applicable).
Please check the document version above.

Scattering of harmonic P1 and SV waves by a shallow lined circular tunnel in a poroelastic half-plane

Qijian Liu [a,b,*], Cheng Yue [a], Mingjuan Zhao [c]

[a] College of Civil Engineering, Hunan University, Changsha, Hunan, 410082, PR China
[b] Key Laboratory of Building Safety and Energy Efficiency of the Ministry of Education, Hunan University, Changsha, Hunan, 410082, PR China
[c] Faculty of Civil Engineering and Geosciences, Delft University of Technology, 2600 GA, Delft, the Netherlands

ARTICLE INFO

ABSTRACT

An analytical solution for the scattering of harmonic P1 and SV waves in a poroelastic half-plane with a shallow lined tunnel is obtained using the plane complex theory in elastodynamics. In light of the wave function expansions, the wave fields of the poroelastic medium and the liner with unknown coefficients are obtained based on Biot's theory and Helmholtz decomposition. Complex-valued expressions of the effective stresses, the fluid stress, and the displacements of the poroelastic medium and the liner are expressed by the complex variable function method and the conformal transformation technique. With the boundary conditions and the continuity of the medium-liner interface, the boundary value problem results in a series of algebraic equations. The unknown coefficients in the infinite set of algebraic equations can be solved numerically by truncating the series number. A parametric study for the incident SV waves is performed to investigate dynamic stress concentrations and fluid stress of the medium and the liner. Numerical results show that the embedment depth of the tunnel, the incident angle of the excitations, and the porosity of the medium have considerable influence on the dynamic responses of the medium and the liner. The shielding effect of the tunnel on the incident SV waves is obvious. For the big embedment depth of the tunnel, the scattered waves contribute little to the displacements and dynamic stress concentration of the medium and the liner. For a high porosity close to the critical value, the response of the medium-liner system to the incident waves is great.

1. Introduction

Scattering of earthquake waves by embedded inclusions or local topographies in a half-plane is a very important topic in seismology, geotechnical engineering, and acoustics. Site investigations and theoretical studies indicate that additional dynamic stresses and displacements may occur due to the scattering of the incident and reflected waves by the embedded inclusions [1–3]. In order to simulate the scattering of waves in an elastic half-plane by the inclusions, a lot of literatures have been devoted in the latest decades by either analytical or numerical schemes. In the numerical solutions, the boundary element method (BEM) is widely used for the scattering of stress waves since the far-field radiation condition can be automatically satisfied [4–15].

In contrast to numerical methods, analytical solutions are limited to treating the linear elastodynamics with simple geometry. However, analytical solutions are served as the benchmark of the numerical methods as they are closed-form and require less numerical

implementation. The precise analytical solutions for the scattering of elastic waves in a half-plane with a circular cavity may be early presented by Gregory [16,17] and Martin [18,19]. Their results contain the singular integrals of the displacements and stresses of the medium, which are extremely difficult to be implemented. Later, Lin et al. [20] presented an analytical method to examine the zero-stress cylindrical wave functions around a circular cavity in a flat and elastic half-space. Apart from the precise solutions, the approximate analytical method is widely used to deal with the scattering of plane waves by a cavity in an elastic and poroelastic half-plane [21–31]. The key of the approximation is the replacing of the half surface with a convex or concave circular surface by a large radius. The large circular-arc approximation proposed firstly by Lee and Cao [21] is very useful and powerful in practical engineering since it simplified easily the transformation between the Cartesian and cylindrical coordinates by Graf's addition theorem. According to the essentials of special functions, the mathematical base of the treatment is the properties of Bessel functions that their values

---

approach zero when their kernels are large numbers [32,33]. Thus, the approximation of the zero-stress boundary conditions to the circle of the large radii indicates the relaxation of the zero-stress field conditions along the half surface. To improve the relaxation, Lin et al. [20] used the Hankel function integral representation to perform the transformation between the Cartesian coordinate and cylindrical coordinate, which was first conducted by Lamb [34]. Lee and Liu [35] re-examined the problem and proposed an analytical solution for the scattering of P and SV waves by a semi-circular canyon in an elastic half-plane. Zhang et al. [36] investigated site amplification of a half-plane with a radially layered circular canyon and a dam by the antiplane waves. Li et al. [37] investigated the scattering and diffraction of the plane SV waves in an undersea lined tunnel by considering the dynamic interactions of fluid-soil-structure couplings.

The dynamic response of a poroelastic half-plane with a shallow tunnel by the incident plane waves has been barely investigated by the analytical method except for the BEM solution [13]. In this paper, an analytical solution for the scattering of waves by an embedded circular lined tunnel in a poroelastic half-plane is presented by the plane complex variable method in elastodynamics. It is noted that the complex variable method was firstly extended to solve the dynamic response of an irregularly shaped cavity in an elastic space by Liu et al. [38]. Recently, the authors analyzed the scattering of earthquake waves by the lined tunnel in an elastic half-plane by using the complex variable method and conformal mapping [39]. The idea will be extended in this study to the scattering of plane waves by a circular lined tunnel in a poroelastic half-plane. The complex variable method and conformal mapping can convert the expressions of the scattered waves from the Cartesian coordinate to the cylindrical coordinate by the Möbius transformation to a concentric ring in the image plane. It is strict mathematically to meet fully the boundary conditions. Moreover, the singular integrals in the solution will be avoided in the method. The present solution is to solve Biot's equations by the Helmholtz decomposition for the poroelastic medium first. In terms of the complex variable method, general complex expressions for the effective stresses, fluid stress, and displacements of the elastic medium and liner are obtained. Then, conformal transformation is adopted to map the medium and the

shallow circular tunnel onto two concentric circles in the image plane. The boundary value problem will be formulated by the boundary conditions and the continuity of the medium-liner interface as an infinite linear algebraic system. Then, a parametric study will be performed to investigate the effects of the embedment depth of the tunnel, the incident angle of the excitations and the porosity of the medium on the dynamic response of the medium-liner system.

2. The model

The cross-section of the two-dimensional problem of concern and the adopted coordinate systems are shown in Fig. 1. The fluid-saturated medium is homogenous, isotropic, and linearly elastic, which is simulated by Biot's two-phase theory. The circular lined tunnel with inner radius R_1 and outer radius R_2 is located at depth h below the half surface. The liner is assumed to be elastic with Lamé constants λ_2 and μ_2 and density ρ_2, respectively. The incident P1 and SV excitations are assumed to be harmonic with angle γ and the circular frequency ω. The harmonic time unit $e^{-i\omega t}$ will be understood and omitted in the following analysis. It is also assumed that the medium-liner interface is perfectly jointed, which indicates that there is no slippage at the interface.

3. Biot's theory for the poroelastic media

Based on Biot's theory [40], the equations of motion expressed by the solid displacement vector $\mathbf{u}$ and the displacement vector $\mathbf{U}$ for the pore fluid are

$$\mu_1 \nabla^2 \mathbf{u} + \text{grad}[(\lambda_1 + \mu_1)e + Q\epsilon] = \frac{\partial^2}{\partial t^2}(\rho_{11}\mathbf{u} + \rho_{12}\mathbf{U}) + b\frac{\partial}{\partial t}(\mathbf{u} - \mathbf{U}) \quad (1)$$

$$\text{grad}[Qe + P\epsilon] = \frac{\partial^2}{\partial t^2}(\rho_{12}\mathbf{u} + \rho_{22}\mathbf{U}) - b\frac{\partial}{\partial t}(\mathbf{u} - \mathbf{U}) \quad (2)$$

where $e = \text{div}\mathbf{u}$ and $\epsilon = \text{div}\mathbf{U}$ are the dilatations in the solid matrix and fluid, respectively; λ_1 and μ_1 denote Lamé moduli of the saturated medium; Q and P are the measures of the elastic moduli; b is the dissipative coefficient; ρ_{11}, ρ_{12} and ρ_{22} are dynamic effective mass coefficients,
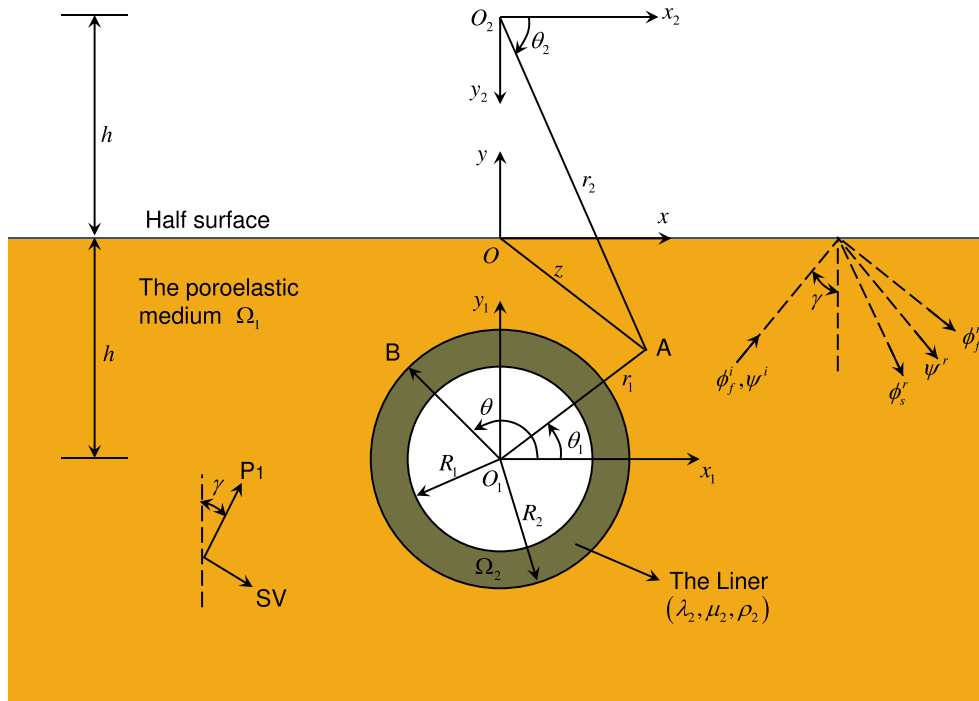

Fig. 1. The shallow circular tunnel in the poroelastic medium by the plane waves.

which can be defined by [42].

$$\rho_{11} = (1-n)\rho_g + \widehat{\gamma}(1-n)\rho_f \tag{3}$$

$$\rho_{12} = -\widehat{\gamma}(1-n)\rho_f \tag{4}$$

$$\rho_{22} = n\rho_f + \widehat{\gamma}(1-n)\rho_f \tag{5}$$

where n is porosity; ρ_g is the density of the solid material; ρ_f is the density of the fluid; $\widehat{\gamma}$ is the coefficient of induced inertia by solid-fluid interaction, which depends on the shape of the solid particles. When the solid skeletons are modeled as spherical particles, $\widehat{\gamma} = 0.5$ [42].

The elastic moduli have been correlated by Biot and Wills [44] based on experimental measurements, which is supposed to be

$$Q = \frac{n\left(1 - n - K_{dry}/K_g\right)}{\left(1 - n - K_{dry}/K_g\right) + nK_g/K_f}K_g \tag{6}$$

$$P = \frac{n^2}{\left(1 - n - K_{dry}/K_g\right) + nK_g/K_f}K_g \tag{7}$$

$$\lambda_1 = \frac{3\nu_1}{1 + \nu_1}K_{dry} + \frac{\left(1 - n - K_{dry}/K_g\right)^2}{\left(1 - n - K_{dry}/K_g\right) + nK_g/K_f}K_g \tag{8}$$

$$\mu_1 = \frac{3(1 - 2\nu_1)}{2(1 + \nu_1)}K_{dry} \tag{9}$$

where ν_1 is the Poisson's ratio of the dry frame; K_g is the bulk modulus of a solid grain; K_f is the bulk modulus of fluid; K_{dry} is the bulk modulus of the frame and can be expressed as [45].

$$K_{dry} = K_{cr} + (1 - n/n_{cr})(K_g - K_{cr}) \tag{10}$$

where n_{cr} is the critical porosity; K_{cr} is the critical bulk modulus for the dry frame.

The stress-strain relationships of the saturated medium are [40].

$$\sigma_{ij} = (\lambda_1 e + Q\epsilon)\delta_{ij} + 2\mu_1 e_{ij} \tag{11}$$

$$p_f = Qe + P\epsilon \tag{12}$$

where σ_{ij} and e_{ij} denote the effective stress and strain tensors in the solid, respectively; δ_{ij} is the Kronecker delta; p_f is the fluid stress.

The stress due to the deformation of the solid skeleton is nominated as the effective stress, and practically denoted as σ_{ij}. The total stress $\widehat{\sigma}_{ij}$ is considered to be composed of the fluid stress and the effective stress in the medium as follow

$$\widehat{\sigma}_{ij} = \sigma_{ij} - np_p\delta_{ij} = \sigma_{ij} + p_f\delta_{ij} \tag{13}$$

where $p_p = -p_f/n$ denotes the pore pressure of the medium [49].

4. Potential functions and the governing equations for the poroelastic media

The Helmholtz decomposition of the displacement vector is applied to solve the equation of motion for the case of small, two-dimensional and time-harmonic vibration of a homogeneous poroelastic continuum. Thus, the displacements fields $\mathbf{u}$ and $\mathbf{U}$ can be resolved by a pair of a scalar potential and a vector potential, which are respectively denoted as φ and ψ for the solid components and H and G for the fluid as

$$\mathbf{u} = \nabla\varphi + \nabla \times \psi \tag{14}$$

$$\mathbf{U} = \nabla H + \nabla \times G \tag{15}$$

Substituting the above decomposition into the wave motion equations by Eq. (1) and Eq. (2), the following Helmholtz equations can be obtained about the scalar potentials φ_f and φ_s, and vector potential ψ_1

$$\nabla^2\varphi_f + k_f^2\varphi_f = 0 \tag{16}$$

$$\nabla^2\varphi_s + k_s^2\varphi_s = 0 \tag{17}$$

$$\nabla^2\psi_1 + k_t^2\psi_1 = 0 \tag{18}$$

where φ_f and φ_s are the longitudinal potentials corresponding to the fast and slow P waves; $\varphi = \varphi_f + \varphi_s$; k_f, k_s and k_t denote the complex wavenumbers of the fast longitudinal wave, the slow longitudinal wave and the transverse wave and can be obtained by [43].

$$k_{f,s}^2 = \frac{B \mp \sqrt{B^2 - 4AC}}{2A} \tag{19}$$

$$k_t^2 = \frac{C}{D} \tag{20}$$

where

$$A = (\lambda_1 + 2\mu_1)P - Q^2 \tag{21}$$

$$B = \omega^2[\rho_{11}P + \rho_{22}(\lambda_1 + 2\mu_1) - 2\rho_{12}Q] + i\omega b(\lambda_1 + 2\mu_1 + 2Q + P) \tag{22}$$

$$C = \omega^2\left[\omega^2\left(\rho_{11}\rho_{22} - \rho_{12}^2\right) + i\omega\rho_1 b\right] \tag{23}$$

$$D = \mu_1\left[\rho_{22}\omega^2 + i\omega b\right] \tag{24}$$

where $\rho_1 = (1-n)\rho_g + n\rho_f$ is the total density of the medium; b is a viscous coupling factor [43].

Furthermore, the potentials H and G can be derived as

$$H = \mu_f\varphi_f + \mu_s\varphi_s \tag{25}$$

$$G = \mu_t\psi_1 \tag{26}$$

where

$$\mu_{f,s} = \frac{\omega^2(\rho_{11}P - \rho_{12}Q) - k_{f,s}^2\left[(\lambda_1 + 2\mu_1)P - Q^2\right] + i\omega b(Q + P)}{\omega^2(\rho_{22}Q - \rho_{12}P) + i\omega b(Q + P)} \tag{27}$$

$$\mu_t = -\frac{\omega^2\rho_{12} - i\omega b}{\omega^2\rho_{22} + i\omega b} \tag{28}$$

5. Total wave potentials of the medium and the liner

5.1. Wave potentials of the poroelastic medium

5.1.1. Wave potentials of the free field

5.1.1.1. Incident P waves.
For the obliquely incident P waves with angle γ and the amplitude φ_{f0}, the fast potentials are mostly considered in practical engineering [45]. In this case, the incident potentials φ_f^i, the reflected fast and slow P waves, φ_f^r and φ_s^r, and the reflected SV waves ψ^r can be expressed as

$$\varphi_f^i = \varphi_{f0}\exp\left[ik_f(x\sin\gamma + y\cos\gamma)\right] \tag{29}$$

$$\varphi_f^r = a_{f1}\exp\left[ik_f(x\sin\gamma - y\cos\gamma)\right] \tag{30}$$

$$\varphi_s^r = a_{f2}\exp[ik_s(x\sin\theta_{\alpha 1} - y\cos\theta_{\alpha 1})] \tag{31}$$

$$\psi^r = b_{f1}\exp\left[ik_t(x\sin\theta_{\beta 1} - y\cos\theta_{\beta 1})\right] \tag{32}$$

where $\theta_{\alpha 1} = \arcsin(k_f\sin\gamma/k_s)$; $\theta_{\beta 1} = \arcsin(k_f\sin\gamma/k_t)$; a_{f1}, a_{f2} and b_{f1} are the coefficients satisfying the traction-free boundary conditions at the saturated half-plane [45].

5.1.1.2. Incident SV waves. For incident SV wave with amplitude ψ_0, three cases occur potentially according to the comparison of the incident angle γ with the so-called critical angles θ_{cr1} and θ_{cr2}, which are defined as

$$\theta_{cr1} = \arcsin\left(k_f / k_t\right) \tag{33}$$

$$\theta_{cr2} = \arcsin\left(k_s / k_t\right) \tag{34}$$

Case I. $\gamma \leq \theta_{cr1}$

In this case, the incident potentials ψ_f^i of the amplitude ψ_0 and the reflected fast and slow P waves φ_f^r and φ_s^r, and the reflected SV waves ψ^r can be respectively expressed as

$$\psi^i = \psi_0 \exp[ik_t(x\sin\gamma + y\cos\gamma)] \tag{35}$$

$$\varphi_f^r = a_{t1}\exp\left[ik_f(x\sin\theta_{\alpha3} - y\cos\theta_{\alpha3})\right] \tag{36}$$

$$\varphi_s^r = a_{t2}\exp\left[ik_s(x\sin\theta_{\beta3} - y\cos\theta_{\beta3})\right] \tag{37}$$

$$\psi^r = b_{t1}\exp[ik_t(x\sin\gamma - y\cos\gamma)] \tag{38}$$

where $\theta_{\alpha3} = \arcsin(k_t\sin\gamma/k_f)$; $\theta_{\beta3} = \arcsin(k_t\sin\gamma/k_s)$; a_{t1}, a_{t2} and b_{t1} are the coefficients satisfying the traction-free boundary conditions at the saturated half-plane [45].

Case II. $\gamma \geq \theta_{cr1}$

When the incident angle reaches the first critical angle θ_{cr1}, the reflected fast P wave turns to be surface waves and the reflected angle $\theta_{\alpha3}$ turns to $90°$. The reflected slow P wave is described by Eq. (37), whereas the surface wave is given as [39].

$$\varphi_f^r = a_{t1}\exp[ikx - \gamma_1 y] \tag{39}$$

where a_{t1} is the coefficient of the surface wave which can be get from the traction-free condition, $k = k_t\sin\gamma = k_f\sin\theta_{\alpha3} = k_s\sin\theta_{\beta3}$ is the apparent wave-number, and

$$\gamma_1 = ik_f\cos\theta_{\alpha3} = -\sqrt{k^2 - k_f^2} \tag{40}$$

Case III. $\gamma \geq \theta_{cr2}$ In unconsolidated soft solid frame, the velocity of the slow P waves is greater than that of the SV waves. When the incident angle reaches the second critical angle θ_{cr2}, the reflected slow P waves turns to be surface waves and the reflected angle $\theta_{\beta3}$ turns to $90°$. The surface wave transformed from the slow P wave is given as [41].

$$\varphi_s^r = a_{t2}\exp[ikx - \gamma_2 y] \tag{41}$$

where a_{t2} is the coefficient of the surface wave which can be get from the traction-free condition, k is the apparent wave-number, and

$$\gamma_2 = ik_s\cos\theta_{\beta3} = -\sqrt{k^2 - k_s^2} \tag{42}$$

5.1.2. The scattered potentials

In the poroelastic half-plane, for the presence of the circular tunnel, the incident and the reflected waves will be scattered around the tunnel. The scattered waves should satisfy the equation of motion and Sommerfeld's radiation conditions [46,47]. Therefore, the scattered waves by the tunnel and the half surface should be outgoing while not ingoing. The scattered P and SV waves are generated at the cavity are represented by φ_{f1}^s, φ_{s1}^s and ψ_1^s. Due to the vibrations of the circular cavity, the scattered wave φ_{f1}^s, φ_{s1}^s and ψ_1^s are reflected off the half surface and new waves are generated and can be represented by φ_{f2}^s, φ_{s2}^s and ψ_2^s,

respectively. Therefore, the scattered waves φ_{f2}^s, φ_{s2}^s and ψ_2^s can be simulated as scattering from origin O_2, the image of origin O_1. Accordingly, the scattered potentials φ_{f1}^s, φ_{s1}^s and ψ_1^s can be written as

$$\varphi_{f1}^s = \sum_{n=-\infty}^{\infty} a_n H_n^{(1)}\left(k_f r_1\right)e^{in\theta_1} \tag{43}$$

$$\varphi_{s1}^s = \sum_{n=-\infty}^{\infty} b_n H_n^{(1)}(k_s r_1)e^{in\theta_1} \tag{44}$$

$$\psi_1^s = \sum_{n=-\infty}^{\infty} c_n H_n^{(1)}(k_t r_1)e^{in\theta_1} \tag{45}$$

The additional scattered wave potentials φ_{f2}^s, φ_{s2}^s and ψ_2^s at the half surface can be expressed as

$$\varphi_{f2}^s = \sum_{n=-\infty}^{\infty} d_n H_n^{(1)}\left(k_f r_2\right)e^{in\theta_2} \tag{46}$$

$$\varphi_{s2}^s = \sum_{n=-\infty}^{\infty} e_n H_n^{(1)}(k_s r_2)e^{in\theta_2} \tag{47}$$

$$\psi_2^s = \sum_{n=-\infty}^{\infty} f_n H_n^{(1)}(k_t r_2)e^{in\theta_2} \tag{48}$$

where $H_n^{(1)}(\cdot)$ denotes the Hankel function of first kind and order n; a_n, b_n, c_n, d_n, e_n, and f_n are arbitrary coefficients; r_1 and r_2 are norms of vectors $\overrightarrow{O_1A}$ and $\overrightarrow{O_2A}$, respectively (see Fig. 1); θ_1 and θ_2 are the polar coordinate angles shown in Fig. 1 and can be calculated by

$$e^{i\theta_1} = \frac{\overrightarrow{O_1A}}{\left|\overrightarrow{O_1A}\right|} = \frac{z + ih}{|z + ih|} \tag{49}$$

$$e^{i\theta_2} = \frac{\overrightarrow{O_2A}}{\left|\overrightarrow{O_2A}\right|} = \frac{\bar{z} + ih}{|\bar{z} + ih|} \tag{50}$$

Due to the scattering theory of earthquake waves in the elastodynamics, there are three kinds of field potentials in formation, the incident, reflected and scattered wave potentials, respectively. The total wave potentials of the medium are the sum of the incident, reflected and scattered waves, which can be written as

$$\varphi_f = \varphi_f^i + \varphi_f^r + \varphi_{f1}^s + \varphi_{f2}^s \tag{51}$$

$$\varphi_s = \varphi_s^i + \varphi_s^r + \varphi_{s1}^s + \varphi_{s2}^s \tag{52}$$

$$\psi_1 = \psi^i + \psi^r + \psi_1^s + \psi_2^s \tag{53}$$

5.2. Wave potentials of the liner

In the lined tunnel, scattered wave potentials occur due to the vibration of the poroelastic medium. The total wave fields φ_2 and ψ_2 are expressed as [39].

$$\varphi_2 = \sum_{n=-\infty}^{\infty} \left[g_n H_n^{(1)}(k_{L2} r_1) + h_n H_n^{(2)}(k_{L2} r_1)\right]e^{in\theta_1} \tag{54}$$

$$\psi_2 = \sum_{n=-\infty}^{\infty} \left[i_n H_n^{(1)}(k_{T2} r_1) + j_n H_n^{(2)}(k_{T2} r_1)\right]e^{in\theta_1} \tag{55}$$

where $k_{L2} = \omega/c_{L2}$ and $k_{T2} = \omega/c_{T2}$ are the wave-numbers of P and SV waves of the liner, respectively; $c_{L2} = \sqrt{(\lambda_2 + 2\mu_2)/\rho_2}$ and $c_{T2} = \sqrt{\mu_2/\rho_2}$ are the wave velocities of P and SV waves, respectively; $H_n^{(2)}(\cdot)$ denotes the Hankel function of second kind and order n; g_n, h_n, i_n, and j_n are the unknown coefficients to be determined.

6. Complex-valued expressions of the effective stresses, displacements and fluid stress

6.1. The conformal mapping functions

The mapping technique will be adopted to transform the physical

region onto the image region by variables $\zeta = \xi + i\eta$ and $\bar{\zeta} = \xi - i\eta$. As for the poroelastic medium, a Möbius transformation is introduced to map region Ω_1 in Fig. 1 onto a ring region Γ_1 in ζ plane (see Fig. 2) [48].

$$z_1 = w_1(\zeta) = -it\frac{1+\zeta}{1-\zeta} \tag{56}$$

where $t = h(1 - \alpha^2)/(1 + \alpha^2)$; $\alpha = h/R_2 - \sqrt{(h - R_2)^2 - 1}$.

For the liner, different mapping function $w_2(\zeta)$ is applied to map region Ω_2 (see Fig. 1) onto a ring region Γ_2 [39]

$$z_2 = w_2(\zeta) = -ih + \frac{R_2\zeta}{\alpha} \tag{57}$$

This kind of treatment for the problem of concern has been introduced to consider the continuum along with the interface between the elastic medium and the liner. As shown in Fig. 2, it is seen that ring Γ_1, corresponding to the elastic medium, is bounded by two concentric circles, $|\zeta| = \alpha$ and $|\zeta| = 1$, respectively. Likewise, ring Γ_2 is bounded by two concentric circles, $|\zeta| = \alpha$ and $|\zeta| = \alpha_1 = \alpha R_1/R_2$, respectively. There is a jointed boundary $|\zeta| = \alpha$ by regions Γ_1 and Γ_2. Circles $|\zeta| = 1$, $|\zeta| = \alpha$, $|\zeta| = \alpha_1$ in the image domain correspond monotonously to the half surface, the medium-liner interface and the inner surface of the liner, respectively.

6.2. General expressions of the effective stresses and displacements

The displacements of the poroelastic medium expressed by Eqs. (14) and (15) can be converted to the following forms

$$u_1 = \frac{\partial\varphi_f}{\partial x} + \frac{\partial\varphi_s}{\partial x} + \frac{\partial\psi_1}{\partial y} \tag{58}$$

$$v_1 = \frac{\partial\varphi_f}{\partial y} + \frac{\partial\varphi_s}{\partial y} - \frac{\partial\psi_1}{\partial x} \tag{59}$$

$$U_x = \mu_f\frac{\partial\varphi_f}{\partial x} + \mu_s\frac{\partial\varphi_s}{\partial x} + \mu_t\frac{\partial\psi_1}{\partial y} \tag{60}$$

$$U_y = \mu_f\frac{\partial\varphi_f}{\partial y} + \mu_s\frac{\partial\varphi_s}{\partial y} - \mu_t\frac{\partial\psi_1}{\partial x} \tag{61}$$

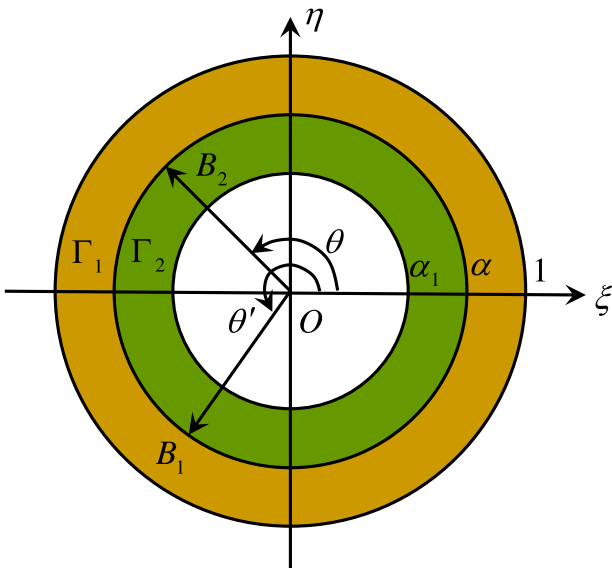Applying the Helmholtz decomposition, the displacement of the liner can be written as

Fig. 2. The geometry of the proposed model [39].

$$u_2 = \frac{\partial\varphi_2}{\partial x} + \frac{\partial\psi_2}{\partial y} \tag{62}$$

$$v_2 = \frac{\partial\varphi_2}{\partial y} - \frac{\partial\psi_2}{\partial x} \tag{63}$$

The complex variables $z = x + iy$ and $\bar{z} = x - iy$ are introduced to transform the expressions of the displacements and effective stresses of the medium. Based on Helmholtz equations and the constitutive model, the combinations of the displacements and stresses of the poroelastic medium can be given as

$$u_1 + iv_1 = 2\frac{\partial}{\partial\bar{z}}(\varphi_f + \varphi_s - i\psi_1) \tag{64}$$

$$u_1 - iv_1 = 2\frac{\partial}{\partial z}(\varphi_f + \varphi_s + i\psi_1) \tag{65}$$

$$u_{r1} + iv_{\theta1} = 2\frac{\partial}{\partial\bar{z}}(\varphi_f + \varphi_s - i\psi_1)e^{-i\chi_1} \tag{66}$$

$$u_{r1} - iv_{\theta1} = 2\frac{\partial}{\partial z}(\varphi_f + \varphi_s + i\psi_1)e^{i\chi_1} \tag{67}$$

$$\Delta_r = u_{r1} - U_r = \frac{\partial}{\partial z}\left(\eta_f\varphi_f + \eta_s\varphi_s + i\eta_t\psi_1\right)e^{i\chi_1}$$
$$+ \frac{\partial}{\partial\bar{z}}\left(\eta_f\varphi_f + \eta_s\varphi_s - i\eta_t\psi_1\right)e^{-i\chi_1} \tag{68}$$

$$\sigma_{y1} + i\sigma_{xy1} = \delta_f\varphi_f + \delta_s\varphi_s - 4\mu_1\frac{\partial^2}{\partial\bar{z}^2}(\varphi_f + \varphi_s + i\psi_1) \tag{69}$$

$$\sigma_{y1} - i\sigma_{xy1} = \delta_f\varphi_f + \delta_s\varphi_s - 4\mu_1\frac{\partial^2}{\partial\bar{z}^2}(\varphi_f + \varphi_s - i\psi_1) \tag{70}$$

$$\sigma_{r1} + i\sigma_{r\theta1} = \delta_f\varphi_f + \delta_s\varphi_s + 4\mu_1\frac{\partial^2}{\partial\bar{z}^2}(\varphi_f + \varphi_s - i\psi_1)e^{-2i\chi_1} \tag{71}$$

$$\sigma_{r1} - i\sigma_{r\theta1} = \delta_f\varphi_f + \delta_s\varphi_s + 4\mu_1\frac{\partial^2}{\partial\bar{z}^2}(\varphi_f + \varphi_s + i\psi_1)e^{2i\chi_1} \tag{72}$$

$$p_f = -\alpha_f k_f^2\varphi_f - \alpha_s k_s^2\varphi_s \tag{73}$$

where $\alpha_{f,s} = Q + \mu_{f,s}P$; $\delta_{f,s} = [n(Q + \mu_{f,s}P) - (\lambda_1 + \mu_1)]k_{f,s}^2$; $\eta_{f,s,t} = 1 - \mu_{f,s,t}$; χ_1 denotes the rotation angle from the coordinate system xoy to system $\rho o\theta$.

The combinations of the displacement and stress of the liner can be given as

$$u_{r2} + iv_{\theta2} = 2\frac{\partial}{\partial\bar{z}}(\varphi_2 - i\psi_2)e^{-i\chi_2} \tag{74}$$

$$u_{r2} - iv_{\theta2} = 2\frac{\partial}{\partial z}(\varphi_2 + i\psi_2)e^{i\chi_2} \tag{75}$$

$$\sigma_{r2} + i\sigma_{r\theta2} = -(\lambda_2 + \mu_2)k_{L2}^2\varphi_2 + 4\mu_2\frac{\partial^2}{\partial\bar{z}^2}(\varphi_2 - i\psi_2)e^{-2i\chi_2} \tag{76}$$

$$\sigma_{r2} - i\sigma_{r\theta2} = -(\lambda_2 + \mu_2)k_{L2}^2\varphi_2 + 4\mu_2\frac{\partial^2}{\partial\bar{z}^2}(\varphi_2 + i\psi_2)e^{2i\chi_2} \tag{77}$$

The rotating angle χ_i, $(i = 1, 2)$ can be given by the mapping function as

$$e^{i\chi_i} = \frac{\zeta}{\rho}\frac{w_i'(\zeta)}{|w_i'(\zeta)|} \quad (i = 1, 2) \tag{78}$$

where $\zeta = \rho e^{i\theta}$, ρ and θ presents the polar coordinate after conformal mapping.

After conformal mapping, the displacements and effective stresses in z-plane can be rewritten by ζ and $\overline{\zeta}$ as

$$u_1 + iv_1 = 2\frac{1}{\overline{w_1'(\zeta)}}\frac{\partial}{\partial\overline{\zeta}}(\varphi_f + \varphi_s - i\psi_1) \tag{79}$$

$$u_1 - iv_1 = 2\frac{1}{w_1'(\zeta)}\frac{\partial}{\partial\zeta}(\varphi_f + \varphi_s + i\psi_1) \tag{80}$$

$$u_{r1} + iv_{\theta1} = 2\frac{\overline{\zeta}}{\rho|w_1'(\zeta)|}\frac{\partial}{\partial\overline{\zeta}}(\varphi_f + \varphi_s - i\psi_1) \tag{81}$$

$$u_{r1} - iv_{\theta1} = 2\frac{\zeta}{\rho|w_1'(\zeta)|}\frac{\partial}{\partial\zeta}(\varphi_f + \varphi_s + i\psi_1) \tag{82}$$

$$\begin{aligned}\triangle_r = u_{r1} - U_r &= \frac{\zeta}{\rho|w_1'(\zeta)|}\frac{\partial}{\partial\zeta}(\eta_f\varphi_f + \eta_s\varphi_s + i\eta_t\psi_1)\\ &+ \frac{\overline{\zeta}}{\rho|w_1'(\zeta)|}\frac{\partial}{\partial\overline{\zeta}}(\eta_f\varphi_f + \eta_s\varphi_s - i\eta_t\psi_1)\end{aligned} \tag{83}$$

$$\begin{aligned}\sigma_{y1} + i\sigma_{xy1} &= \delta_f\varphi_f + \delta_s\varphi_s\\ &-4\mu_1\frac{1}{w_1'(\zeta)}\frac{\partial}{\partial\zeta}\left[\frac{1}{\overline{w_1'(\zeta)}}\frac{\partial}{\partial\overline{\zeta}}\left(\varphi_f + \varphi_s + i\psi_1\right)\right]\end{aligned} \tag{84}$$

$$\begin{aligned}\sigma_{y1} - i\sigma_{xy1} &= \delta_f\varphi_f + \delta_s\varphi_s\\ &-4\mu_1\frac{1}{\overline{w_1'(\zeta)}}\frac{\partial}{\partial\overline{\zeta}}\left[\frac{1}{w_1'(\zeta)}\frac{\partial}{\partial\zeta}\left(\varphi_f + \varphi_s - i\psi_1\right)\right]\end{aligned} \tag{85}$$

$$\begin{aligned}\sigma_{r1} + i\sigma_{r\theta1} &= \delta_f\varphi_f + \delta_s\varphi_s\\ &+4\mu_1\frac{\overline{\zeta}^2}{\rho^2}\frac{1}{w_1'(\zeta)}\frac{\partial}{\partial\zeta}\left[\frac{1}{\overline{w_1'(\zeta)}}\frac{\partial}{\partial\overline{\zeta}}\left(\varphi_f + \varphi_s - i\psi_1\right)\right]\end{aligned} \tag{86}$$

$$\begin{aligned}\sigma_{r1} - i\sigma_{r\theta1} &= \delta_f\varphi_f + \delta_s\varphi_s\\ &+4\mu_1\frac{\zeta^2}{\rho^2}\frac{1}{\overline{w_1'(\zeta)}}\frac{\partial}{\partial\overline{\zeta}}\left[\frac{1}{w_1'(\zeta)}\frac{\partial}{\partial\zeta}\left(\varphi_f + \varphi_s + i\psi_1\right)\right]\end{aligned} \tag{87}$$

$$p_f = -\alpha_f k_f^2\varphi_f - \alpha_s k_s^2\varphi_s \tag{88}$$

$$u_{r2} + iv_{\theta2} = 2\frac{\overline{\zeta}}{\rho|w_2'(\zeta)|}\frac{\partial}{\partial\overline{\zeta}}(\varphi_2 - i\psi_2) \tag{89}$$

$$u_{r2} - iv_{\theta2} = 2\frac{\zeta}{\rho|w_2'(\zeta)|}\frac{\partial}{\partial\zeta}(\varphi_2 + i\psi_2) \tag{90}$$

$$\begin{aligned}\sigma_{r2} + i\sigma_{r\theta2} &= -(\lambda_2 + \mu_2)k_{L2}^2\varphi_2\\ &+4\mu_2\frac{\overline{\zeta}^2}{\rho^2}\frac{1}{w_2'(\zeta)}\frac{\partial}{\partial\zeta}\left[\frac{1}{\overline{w_2'(\zeta)}}\frac{\partial}{\partial\overline{\zeta}}(\varphi_2 - i\psi_2)\right]\end{aligned} \tag{91}$$

$$\begin{aligned}\sigma_{r2} - i\sigma_{r\theta2} &= -(\lambda_2 + \mu_2)k_{L2}^2\varphi_2\\ &+4\mu_2\frac{\zeta^2}{\rho^2}\frac{1}{\overline{w_2'(\zeta)}}\frac{\partial}{\partial\overline{\zeta}}\left[\frac{1}{w_2'(\zeta)}\frac{\partial}{\partial\zeta}(\varphi_2 + i\psi_2)\right]\end{aligned} \tag{92}$$

7. Formulations of the boundary value problem

Along with the half surface, it exhibits traction-free field conditions. It is convenient to present the stress conditions in a Cartesian coordinate system xoy as follows:

$$\sigma_{xy1} = \sigma_{y1} = 0, (y = 0) \tag{93}$$

In addition, the fluid stress for the drained case will vanish. Therefore, the boundary condition results in the form

$$p_f = 0 \tag{94}$$

Along the circumference of the internal surface of the liner, the

stress-free boundary conditions can be expressed as

$$\sigma_{r2} = \sigma_{r\theta2} = 0, (r_1 = R_1) \tag{95}$$

The fluid stress for the drained case along the medium-liner interface will disappear, which remains the same formulation as Eq. (94).

For the undrained case, the displacement $\triangle_r$ of the fluid relative to the solid will be zero

$$\triangle_r = 0 \tag{96}$$

The continuity of the stress and displacement at the medium–liner interface ($r_1 = R_2$) results in

$$u_{r1} = u_{r2} \tag{97}$$

$$v_{\theta1} = v_{\theta2} \tag{98}$$

$$\sigma_{r1} = \sigma_{r2} \tag{99}$$

$$\sigma_{r\theta1} = \sigma_{r\theta2} \tag{100}$$

The boundary value problem can be solved directly if the effective stresses and displacements along the boundary are prescribed. In this article, the stress boundary conditions along with the half surface are

$$\begin{aligned}\sigma_{y1} + i\sigma_{xy1} &= \delta_f\varphi_f + \delta_s\varphi_s\\ &-4\mu_1\frac{1}{w_1'(\zeta)}\frac{\partial}{\partial\zeta}\left[\frac{1}{\overline{w_1'(\zeta)}}\frac{\partial}{\partial\overline{\zeta}}\left(\varphi_f + \varphi_s + i\psi_1\right)\right] = 0\end{aligned} \tag{101}$$

$$\begin{aligned}\sigma_{y1} - i\sigma_{xy1} &= \delta_f\varphi_f + \delta_s\varphi_s\\ &-4\mu_1\frac{1}{\overline{w_1'(\zeta)}}\frac{\partial}{\partial\overline{\zeta}}\left[\frac{1}{w_1'(\zeta)}\frac{\partial}{\partial\zeta}\left(\varphi_f + \varphi_s - i\psi_1\right)\right] = 0\end{aligned} \tag{102}$$

Substituting Eq. (88) into Eq. (94), we obtain the boundary condition of the fluid stress along the half surface for the drained case

$$p_f = -\alpha_f k_f^2\varphi_f - \alpha_s k_s^2\varphi_s = 0 \tag{103}$$

Along the circumference of the internal surface of the liner, the stress-free boundary conditions are

$$\begin{aligned}\sigma_{r2} + i\sigma_{r\theta2} &= -(\lambda_2 + \mu_2)k_{L2}^2\varphi_2\\ &+4\mu_2\frac{R_2^2\overline{\zeta}^2}{R_1^2\alpha^2}\frac{1}{w_2'(\zeta)}\frac{\partial}{\partial\zeta}\left[\frac{1}{\overline{w_2'(\zeta)}}\frac{\partial}{\partial\overline{\zeta}}(\varphi_2 - i\psi_2)\right] = 0\end{aligned} \tag{104}$$

$$\begin{aligned}\sigma_{r2} - i\sigma_{r\theta2} &= -(\lambda_2 + \mu_2)k_{L2}^2\varphi_2\\ &+4\mu_2\frac{R_2^2\zeta^2}{R_1^2\alpha^2}\frac{1}{\overline{w_2'(\zeta)}}\frac{\partial}{\partial\overline{\zeta}}\left[\frac{1}{w_2'(\zeta)}\frac{\partial}{\partial\zeta}(\varphi_2 + i\psi_2)\right] = 0\end{aligned} \tag{105}$$

For the drained case, the fluid stress will remain in the form of Eq. (103). On the other hand, the pore boundary condition for the undrained case along with the medium-liner interface can be obtained by substituting Eq. (83) into Eq. (96) as

$$\begin{aligned}\triangle_r &= \frac{\zeta_1}{\alpha|w_1'(\zeta_1)|}\frac{\partial}{\partial\zeta_1}(\eta_f\varphi_f + \eta_s\varphi_s + i\eta_t\psi_1)\\ &+ \frac{\overline{\zeta_1}}{\alpha|w_1'(\zeta_1)|}\frac{\partial}{\partial\overline{\zeta_1}}(\eta_f\varphi_f + \eta_s\varphi_s - i\eta_t\psi_1) = 0\end{aligned} \tag{106}$$

Likewise, substituting Eqs. (81), (82) and (89)–(90) into Eqs. (97) and (98), we obtain

$$\begin{aligned}u_{r1} + iv_{\theta1} &= 2\frac{\overline{\zeta_1}}{\alpha|w_1'(\zeta_1)|}\frac{\partial}{\partial\overline{\zeta_1}}(\varphi_f + \varphi_s - i\psi_1)\\ &= u_{r2} + iv_{\theta2} = 2\frac{\overline{\zeta}}{\alpha|w_2'(\zeta)|}\frac{\partial}{\partial\overline{\zeta}}(\varphi_2 - i\psi_2)\end{aligned} \tag{107}$$

$$\begin{aligned}u_{r1} - iv_{\theta1} &= 2\frac{\zeta_1}{\alpha|w_1'(\zeta_1)|}\frac{\partial}{\partial\zeta_1}(\varphi_f + \varphi_s + i\psi_1)\\ &= u_{r2} - iv_{\theta2} = 2\frac{\zeta}{\alpha|w_2'(\zeta)|}\frac{\partial}{\partial\zeta}(\varphi_2 + i\psi_2)\end{aligned} \tag{108}$$

where $\zeta_1 = \alpha e^{i\theta'}$ denotes the complex argument of point B_1 in the image plane and θ' is the polar angle of ζ_1.

Substituting Eqs. (86)- Eqs. (87) and (91)- (92) into Eqs. (99) and (100) yields

$$\sigma_{r1} + i\tau_{r\theta1} = \delta_f\varphi_f + \delta_s\varphi_s + 4\mu_1\frac{\overline{\zeta_1^2}}{\alpha^2}\frac{1}{w_1'(\zeta_1)}\frac{\partial}{\partial\overline{\zeta_1}}\left[\frac{1}{\overline{w_1'(\zeta_1)}}\frac{\partial}{\partial\overline{\zeta_1}}(\varphi_f + \varphi_s - i\psi_1)\right]$$
$$= \sigma_{r2} + i\tau_{r\theta2} = -(\lambda_2 + \mu_2)k_{L2}^2\varphi_2 + 4\mu_2\frac{\overline{\zeta}^2}{\alpha^2}\frac{1}{w_2'(\zeta)}\frac{\partial}{\partial\overline{\zeta}}\left[\frac{1}{\overline{w_2'(\zeta)}}\frac{\partial}{\partial\overline{\zeta}}(\varphi_2 - i\psi_2)\right]$$

(109)

$$\sigma_{r1} - i\tau_{r\theta1} = \delta_f\varphi_f + \delta_s\varphi_s + 4\mu_1\frac{\zeta_1^2}{\alpha^2}\frac{1}{w_1'(\zeta_1)}\frac{\partial}{\partial\zeta_1}\left[\frac{1}{w_1'(\zeta_1)}\frac{\partial}{\partial\zeta_1}(\varphi_f + \varphi_s + i\psi_1)\right]$$
$$= \sigma_{r2} - i\tau_{r\theta2} = -(\lambda_2 + \mu_2)k_{L2}^2\varphi_2 + 4\mu_2\frac{\zeta^2}{\alpha^2}\frac{1}{w_2'(\zeta)}\frac{\partial}{\partial\zeta}\left[\frac{1}{w_2'(\zeta)}\frac{\partial}{\partial\zeta}(\varphi_2 + i\psi_2)\right]$$

(110)

Because functions $w_1(\zeta)$ by Eq. (56) and $w_2(\zeta)$ by Eq. (57) are different from each other, point at the medium-liner interface will be mapped to different locations on the image plane. For example, point B at the interface in Fig. 1 corresponds to B_2 for the liner and B_1 for the poroelastic medium in the image plane, respectively (see Fig. 2). The polar angle θ of vector $\overrightarrow{OB_2}$ remains the same value of $\overrightarrow{O_1B}$ in Fig. 1. However, the polar angle of vector $\overrightarrow{OB_1}$ is θ' after mapping by Eq. (56) as shown in Fig. 2, which is different from θ. The relationship between θ and θ' is given by

$$\theta'(\theta) = \arg\left[\frac{iR_2e^{i\theta} + h - t}{iR_2e^{i\theta} + h + t}\right]$$

(111)

In Eqs. (101)-(110), it is obvious that u_{r1}, $v_{\theta1}$, σ_{r1} and $\sigma_{r\theta1}$ are functions of θ', while u_{r2}, $v_{\theta2}$, σ_{r2} and $\sigma_{r\theta2}$ are funtions of θ. Substituting Eqs. (51)-(55) into Eqs. (101)-(110) and considering Eqs. (111), we obtain

$$\sum_{i=1}^{10}\sum_{n=-\infty}^{\infty}E_{i,jn}X_n^i = R_j, (j = 1, ..., 10)$$

(112)

where $X_n^1 = a_n$, $X_n^2 = b_n$, $X_n^3 = c_n$, $X_n^4 = d_n$, $X_n^5 = e_n$, $X_n^6 = f_n$, $X_n^7 = g_n$, $X_n^8 = h_n$, $X_n^9 = i_n$, $X_n^{10} = j_n$; $E_{i,jn}$ and R_j are presented in Appendix A.

It shows that $E_{i,jn}$ and R_j are the functions of the polar angele of θ in the image plane. Multiplying both sides of Eqs. (112) with $e^{-is\theta}$ and integrating over the interval $[-\pi, \pi]$, we get

$$\sum_{i=1}^{10}\sum_{n=-\infty}^{\infty}E_{i,jn}^sX_n^i = R_j^s, (j = 1, ..., 10, s = 0, \pm1, \pm2, ...)$$

(113)

where $E_{i,jn}^s = \int_{-\pi}^{\pi}E_{i,jn}e^{-is\theta}d\theta/(2\pi)$ and $R_j^s = \int_{-\pi}^{\pi}R_je^{-is\theta}d\theta/(2\pi)$

Obviously, Eq. (113) contains a set of infinite linear algebraic systems with respect to the unknown expansion coefficients and may be solved straightforwardly. Since the total wave potentials are expressed by the infinite series, the accuracy of the present solution depends greatly on the truncating of order n to N. Therefore, the series number N should be carefully chosen to ensure the convergence and accuracy of the solution. All results can be obtained easily on a desktop computer in 15 s with 3.19 GHz Intel(R) Core(TM) i7-8700 CPU and 32.00 GB RAM under Windows 10 21H1 environment.

8. Validation

To verify the accuracy of the proposed method, comparisons of the results by the present solution with those available methods by the in-direct boundary integral method will be carried out. For the convenience of demonstration, two non-dimensional parameters, the dynamic stress concentration factor $\sigma_{\theta i}^*$ ($i = 1, 2$) (DSCF) in the medium and the liner, and the non-dimensional fluid stress p_f^*, are defined as

$$\sigma_{\theta i}^* = \frac{\sigma_{\theta i}}{\sigma_0}$$

(114)

$$p_f^* = \frac{p_f}{p_0}$$

(115)

where $\sigma_{\theta i}$ is the tangential stress of the medium and liner; $\sigma_0 = \text{Re}[-(\lambda_1 + 2\mu_1)k_f^2\varphi_0]$; $p_0 = \text{Re}[-\alpha_f k_f^2\varphi_{f0}]$.

The tangential stresses of the medium $\sigma_{\theta1}$, the outer and inner surfaces of the liner, $\sigma_{\theta2}^O$ and $\sigma_{\theta2}^I$, are obtained as

$$\sigma_{\theta1} = -(\lambda_1 + \mu_1)\left(k_f^2\varphi_f + k_s^2\varphi_s\right) - (\delta_f\varphi_f + \delta_s\varphi_s)$$
$$-2\mu_1\frac{\overline{\zeta}^2}{\alpha^2}\frac{1}{w_1'(\zeta)}\frac{\partial}{\partial\overline{\zeta}}\left[\frac{1}{\overline{w_1'(\zeta)}}\frac{\partial}{\partial\overline{\zeta}}(\varphi_f + \varphi_s - i\psi_1)\right]$$
$$-2\mu_1\frac{\zeta^2}{\alpha^2}\frac{1}{w_1'(\zeta)}\frac{\partial}{\partial\zeta}\left[\frac{1}{w_1'(\zeta)}\frac{\partial}{\partial\zeta}(\varphi_f + \varphi_s + i\psi_1)\right]$$

(116)

$$\sigma_{\theta2}^O = -(\lambda_2 + \mu_2)k_{L2}^2\varphi_2$$
$$-2\mu_2\frac{\overline{\zeta}^2}{\alpha^2}\frac{1}{w_2'(\zeta)}\frac{\partial}{\partial\overline{\zeta}}\left[\frac{1}{\overline{w_2'(\zeta)}}\frac{\partial}{\partial\overline{\zeta}}(\varphi_2 - i\psi_2)\right]$$
$$-2\mu_2\frac{\zeta^2}{\alpha^2}\frac{1}{w_2'(\zeta)}\frac{\partial}{\partial\zeta}\left[\frac{1}{w_2'(\zeta)}\frac{\partial}{\partial\zeta}(\varphi_2 + i\psi_2)\right]$$

(117)

$$\sigma_{\theta2}^I = -2(\lambda_2 + \mu_2)k_{L2}^2\varphi_2$$

(118)

Fig. 3 shows a comparison of the hoop stresses along the unlined cavity in an elastic half-plane by the proposed solution with those by Luco and de Barros [6] for a vertically incident fast P wave and SV wave ($\gamma = 0$). To match the parameters by Luco and de Barros [6], the following geometric and material properties are adopted: $h = 7.5$ m, $R_1 = 4.99$ m, $R_2 = 5.0$ m, $n_{cr} = 0.36$, $K_{cr} = 50$ MPa, $K_g = 87.02$ MPa, $K_f = 2000$ MPa, $\rho_g = 1932$ kg/m³, $\rho_f = 1000$ kg/m³, $\widehat{\gamma} = 0.5$, $n = 0.0005$, $\nu_1 = 1/3$, $\lambda_2 = 0.67$ MPa, $\mu_2 = 1.0$ MPa, $\rho_2 = 1.0$ kg/m³, $\omega = 40.81$, $b = 0$. From the above parameters, we obtain: $\lambda_1 = 6.52 \times 10^7$Pa, $\mu_1 = 3.26 \times 10^7$Pa, $\rho_1 \approx 1932$ kg/m³. In Fig. 3, $U_{pf} = ik_f\varphi_{f0}$ and $U_s = ik_t\psi_0$. It should be noted that $n = 0.0005$ corresponds to the medium with a very low porosity which can be reduced to the pure elastic medium. Good agreements of the comparisons enhance the accuracy of the proposed approach for scattering of plane waves by the unlined cavity in an elastic half-plane.

Fig. 4 shows a comparison of the displacements along the half surface of the shallow lined tunnel by the proposed solution with those by Liu et al. [13] for an obliquely incident fast P waves ($\gamma = 30°$). The following parameters for the poroelastic medium and the liner are adopted: $h = 30$ m, $R_1 = 10.0$ m, $R_2 = 10.35$ m $n_{cr} = 0.36$, $K_{cr} = 200$ MPa, $K_g = 36000$ MPa, $K_f = 2000$ MPa, $\rho_g = 2650$ kg/m³, $\rho_f = 1000$ kg/m³, $\widehat{\gamma} = 0.5$, $n = 0.3$, $\nu_1 = 0.25$, $b = 0$, $\rho_2 = 2500$ kg/m³, $\lambda_2 = 9583.3$ MPa, $\mu_2 = 14375$ MPa. The comparison indicates that the present results agree well with the indirect boundary element method except for several locations of the surface. It is observed that good agreements in the comparison can be achieved for not only low but also high frequency waves.

9. Results and discussions

In this section, the effects of the embedment depth ratio $\chi = h/R_2$ and the porosity of the medium on the dynamic response of the medium-tunnel system are demonstrated. Permeable hydrodynamic conditions at the half surface and undrained condition along with the medium-liner interface are considered, respectively. If not specifically mentioned, the parameters of the poroelastic medium and the liner are chosen as the same as those in the comparison with Liu et al. [13]. The circular frequency of the vertically incident SV waves is set to be $\omega = 420.973$. The radii of the outer and inner surfaces of the liner are $R_1 = 5.0$ m, $R_2 = 5.35$ m, respectively.
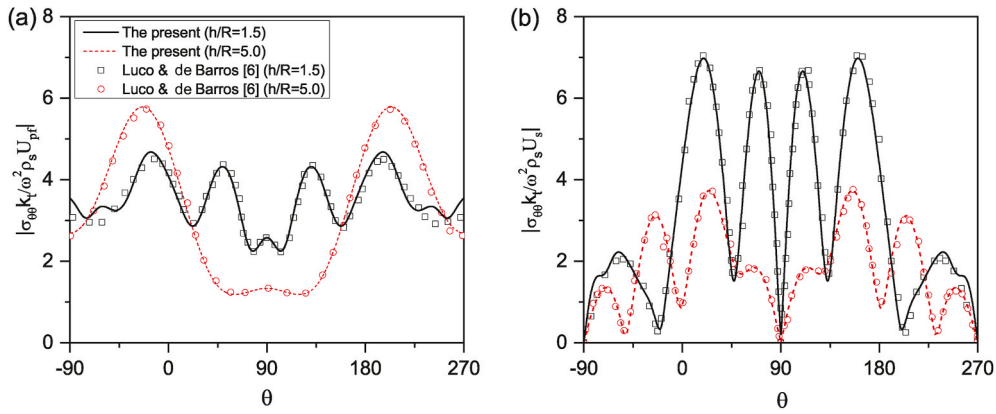
Fig. 3. Comparisons of the present results with those by Luco and de Barros [6] for vertically incident fast P waves (a) and SV-waves (b).
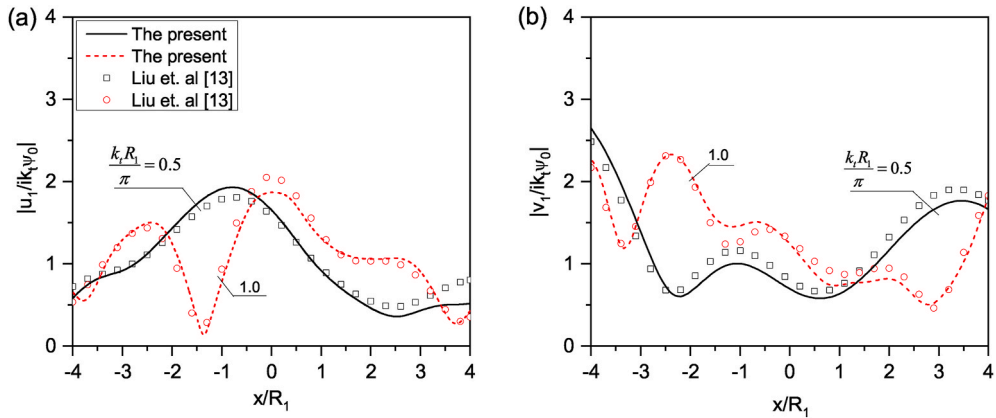

Fig. 4. Comparisons of the present results with those by Liu et al. [13] for obliquely incident P-waves. ($\gamma = 30°$).

9.1. The effect of the liner's embedment depth

9.1.1. Vertical incidence

Fig. 5 shows the displacements at the half surface with different embedment ratios of the liner with $\gamma = 0$. It is seen that the horizontal displacements are larger than the vertical displacements. This can be explained that the response of the medium along with the horizontal direction exhibits intensively because the excitations are vertically incident. Moreover, it indicates that shadows of the half surface behind the liner display resonance and extra displacements occur. Recalling the general understanding that displacements along the half surface caused by the incident and reflected waves are constant, additional

displacements are contributed from the scattered wave potentials by the liner and half surface. When the embedment ratio χ is small, the effect of the scattered waves on the half surface is great. However, the influence of the scattered waves on the half surface turns to be weak when the liner is embedded deeply, resulting in the flat and wide displacement curves correspondingly.

Fig. 6 shows the DSCFs along the cavity of the medium $\sigma_{\theta 1}^*$, and the outer and inner surfaces of the liner, $\sigma_{\theta 2}^{O*}$ and $\sigma_{\theta 2}^{I*}$, and the fluid stress along the outer of the liner, p_f^*, respectively. It is observed that the shapes of DSCFs of $\sigma_{\theta 1}^*$, $\sigma_{\theta 2}^{O*}$ and $\sigma_{\theta 2}^{I*}$ are almost identical for the same embedment ratio. Moreover, the DSCFs along the liner are greater than those along the cavity of the medium. This can be understood that the
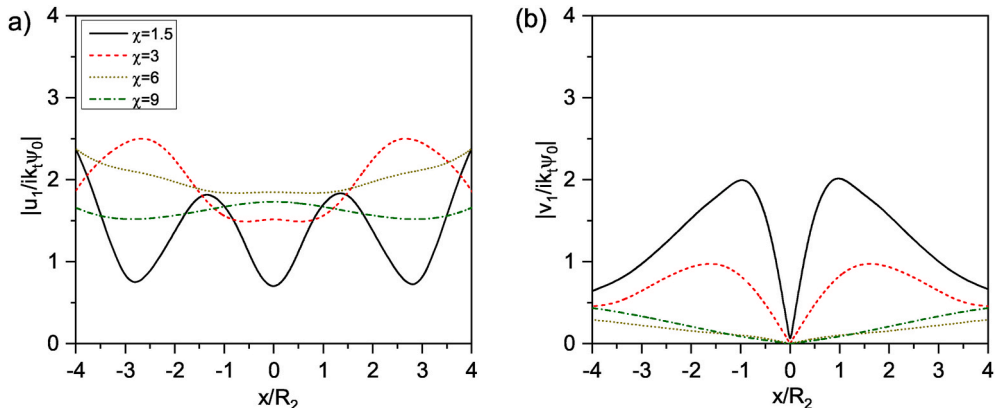

Fig. 5. Horizontal and vertical displacements at half surface by vertically incident SV waves with different χ. $n = 0.3$.
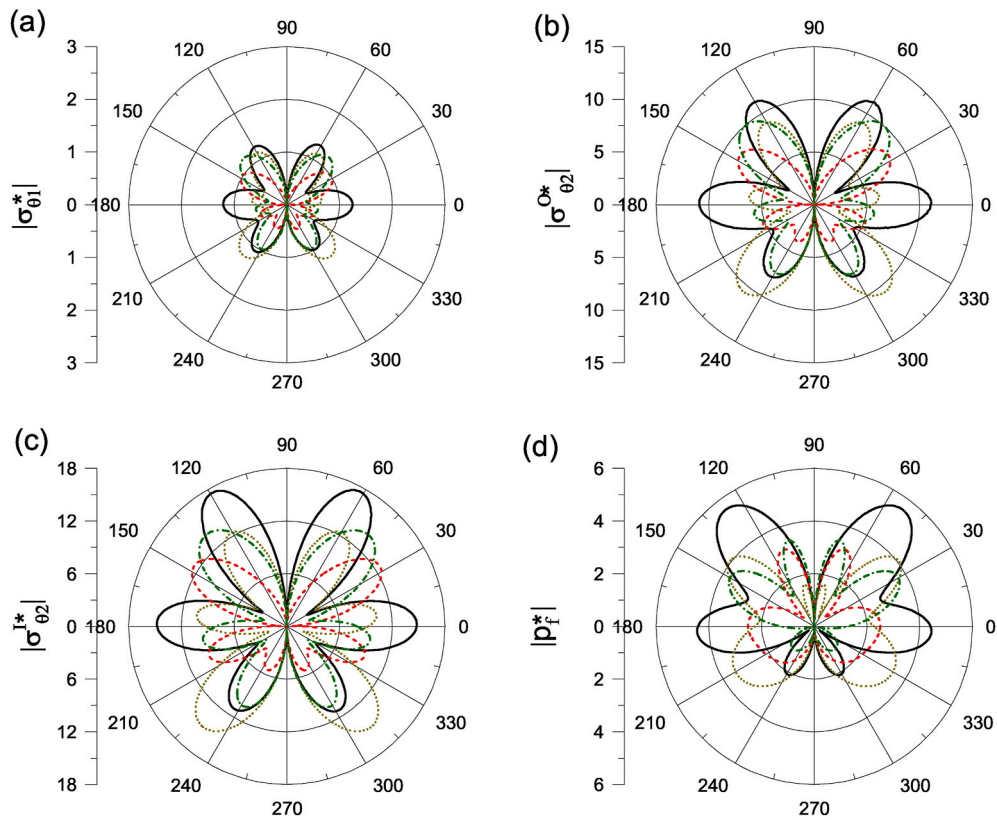
Fig. 6. Distributions of DSCFs and fluid stress by vertically incident SV wave along the cavity and liner with $n = 0.3$. (Solid line, $\chi = 1.5$; dash line, $\chi = 3$; dot line, $\chi = 6$; dash dot line, $\chi = 9$).

big rigidity of the liner in a great response to the incident waves. It is also interesting that the fluid stress at the upper part of the liner are greater than those of the lower part. This is due to the fact that the effect of the scattered waves from the half surface on the upper part of the liner is bigger than that on the lower part.

9.1.2. Oblique incidence

Fig. 7 shows the effect of the obliquely incident angle on the displacements of the half surface to the excitations. It indicates that the influence of the incident angle on the displacements of the half surface is significant compared to Fig. 4. Displacements at the left side of the surface with shallow embedment ratio vibrate frequently. This is understood that the scattered waves from the inclusion contribute much more to the half surface. Moreover, the displacements at the right side of

the half surface turn to be gentle due to the shielding effect of the inclusion to the incident waves. As shown in Fig. 6(b), it is observed the vertical displacements at origin for different embedment ratios are not zero, which is totally different from Fig. 4(b).

Fig. 8 predicted the DSCFs of $\sigma_{\theta1}^*$, $\sigma_{\theta2}^{O*}$, $\sigma_{\theta2}^{I*}$, and p_f^* by obliquely incident SV waves, respectively. It is seen that the response of the medium is weaker than that of the liner. Moreover, resonance occurs in the shadows behind the inclusion along the direction of the incident waves. This can be understood that the scattered waves generate from the half surface contribute greatly to the region of the shadow.

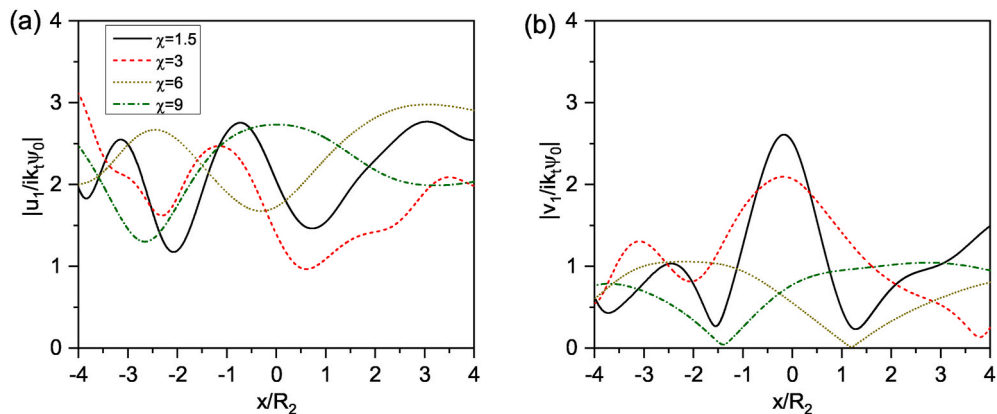**Fig. 7.** Horizontal and vertical displacements by obliquely incident SV wave along the half surface with different embedment depth ratio χ. (Solid line, $\chi = 1.5$; dash line, $\chi = 3$; dot line, $\chi = 6$; dash dot line, $\chi = 9$).
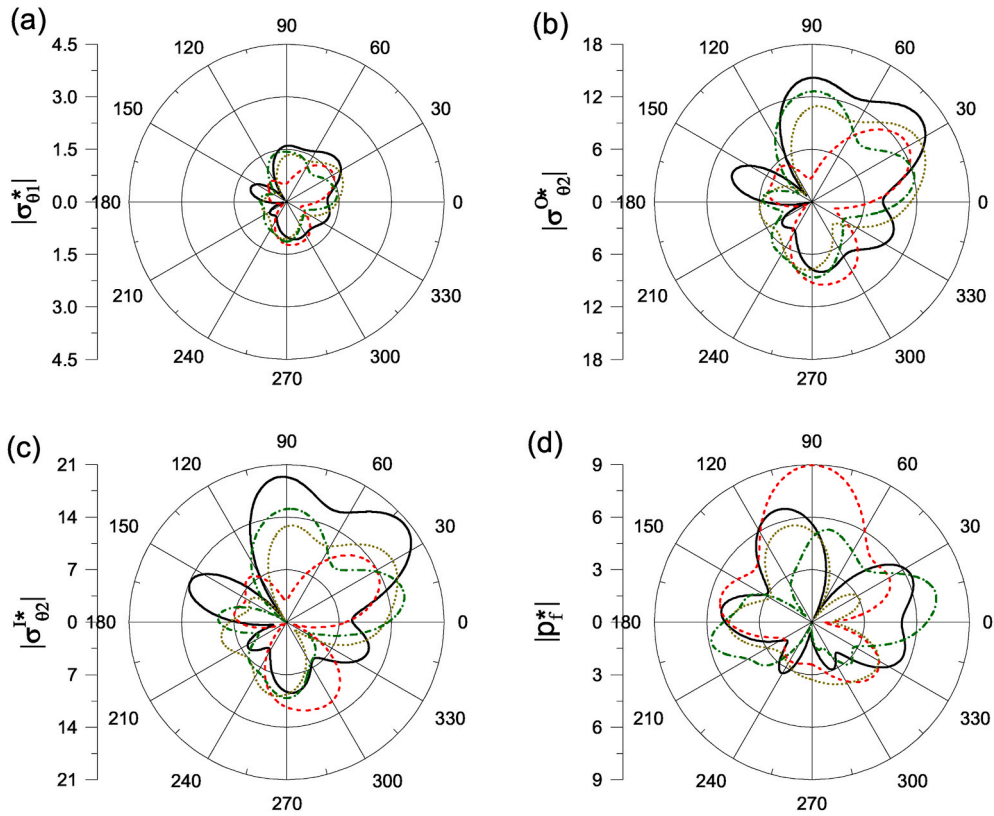
Fig. 8. Distribution of DSCFs and fluid stress by obliquely incident SV wave along the cavity wall with different embedment depth. (Solid line, $\chi = 1.5$; dash line, $\chi = 3$; dot line, $\chi = 6$; dash dot line, $\chi = 9$).

9.2. The effect of the porosity

9.2.1. Vertical incidence

Fig. 9 shows the horizontal and vertical displacements along the half surface with different porosities by vertically incident SV waves. It is seen that the displacements at the half surface within the shadow one time the tunnel radius are almost irrelevant to the porosity when its value is small. However, the effect of the porosity on the horizontal displacements of the half surface is significant for big porosity. It is also interesting that the displacements for very small porosity vibrate frequently along the surface. This can be understood that small porosity results in small wavenumbers of SV waves indicating small wavelength within a given distance.

Fig. 10 shows the DSCFs along the cavity and liner and the fluid stress

for different porosities of the medium. It is seen that dynamic stresses are concentrated mainly at the arch waists of the back of the inclusion to the incident waves. However, different trends of the DSCFs along the cavity of the medium and liner can be observed. With the increase of the porosity, the DSCFs increase in the shadow of the cavity. It is seen that opposite trends can be observed for the liner. The effect of the porosity on the fluid stress in the shadow of the cavity is very similar to that of the DSCFs.

9.2.2. Oblique incidence

Fig. 11 shows the horizontal and vertical displacements along the half surface with different porosities by obliquely incident SV waves. A comparison of Fig. 10 with Fig. 8 indicates that the incident angle has a great influence on the displacements of the half surface. The shielding
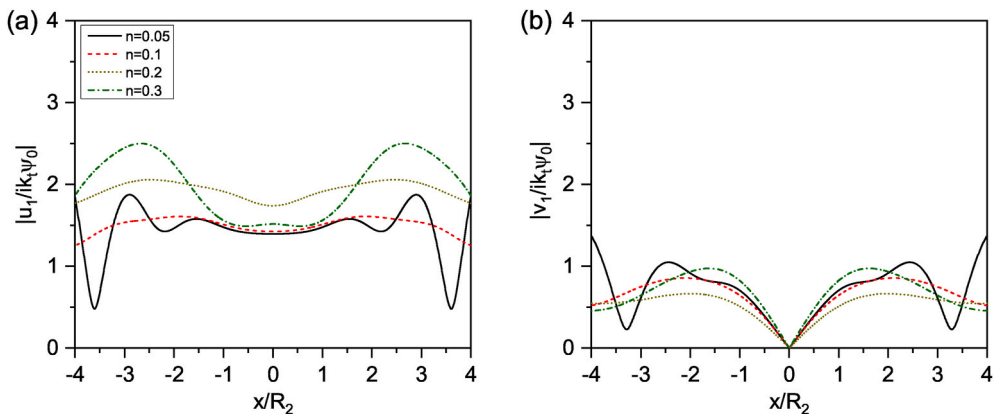

Fig. 9. Horizontal and vertical displacements by vertically incident SV wave along the half surface with different porosity n. (Solid line, $n = 0.05$; dash line, $n = 0.1$; dot line, $n = 0.2$; dash dot line, $n = 0.3$).
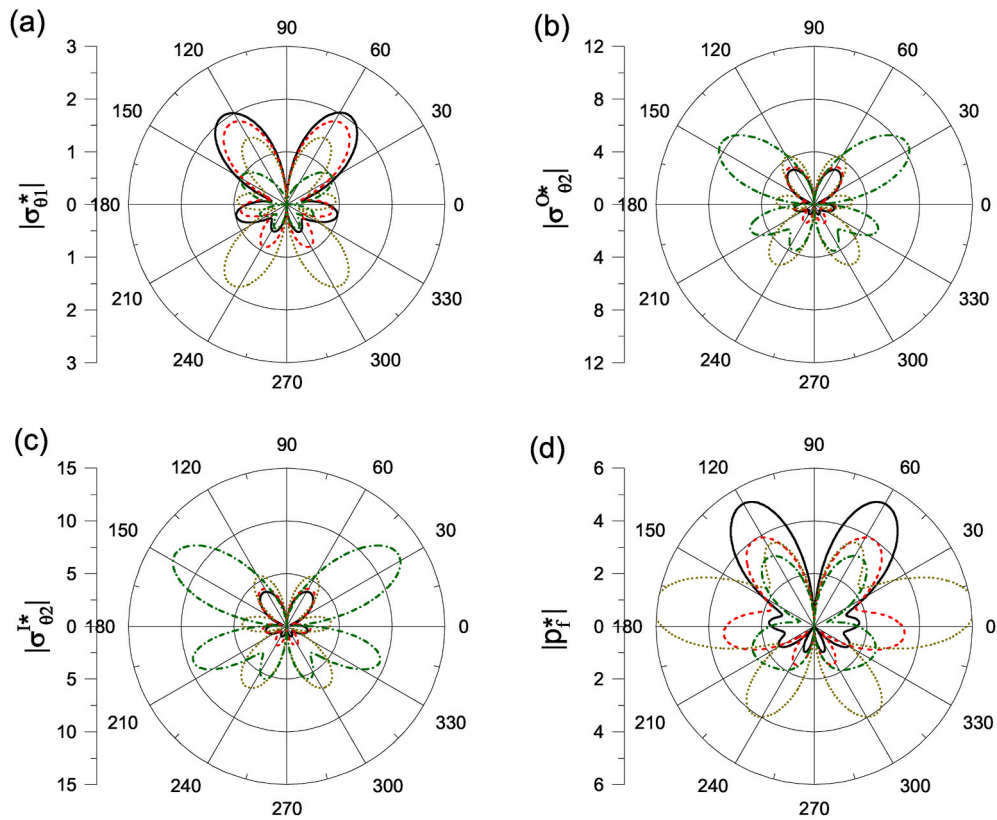
Fig. 10. Distribution of DSCFs and fluid stress by vertically incident SV wave along the cavity wall with different porosity. (Solid line, $n = 0.05$; dash line, $n = 0.1$; dot line, $n = 0.2$; dash dot line, $n = 0.3$).
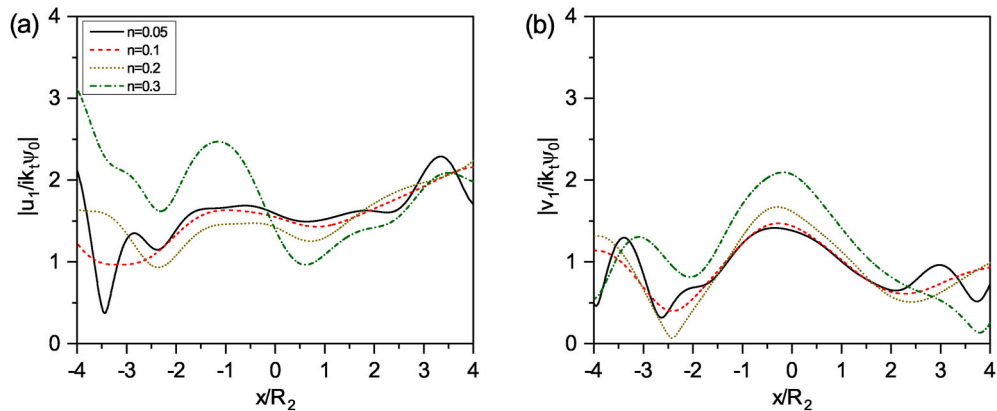

Fig. 11. Horizontal and vertical displacements by obliquely incident SV wave along the half surface with different porosity n. (Solid line, $n = 0.05$; dash line, $n = 0.1$; dot line, $n = 0.2$; dash dot line, $n = 0.3$).

effect of the inclusion to the incident waves is obvious. Moreover, the effect of the porosity on the vertical and horizontal displacements is small. For high porosity $n = 0.3$, displacements on the left side of the surface are large, whereas small on the right side.

Fig. 12 shows the DSCFs of $\sigma_{\theta 1}^*$, $\sigma_{\theta 2}^{O*}$, $\sigma_{\theta 2}^{I*}$, and p_f^* by obliquely incident SV waves with different porosities of the medium, respectively. A similar effect of porosity on DSCFs of $\sigma_{\theta 1}^*$ can be observed as shown in Fig. 10. A high value of porosity $n = 0.3$ has significant influence on the dynamic stress concentration of the cavity. This may be due to the fact that the porosity $n = 0.3$ is very close to the critical porosity $n_{cr} = 0.36$. However, the DSCFs of the outer and inner surfaces of the liner increase with the increase of the porosity. Moreover, the shapes of $\sigma_{\theta 2}^{O*}$ and $\sigma_{\theta 2}^{I*}$ are basically identical though the amplitudes of the inner part are greater than

those of the outer. The response of the liner is greater than that of the medium. Furthermore, it is seen that great fluid stress occur in the shadow behind the tunnel along the direction of the incident waves.

10. Conclusions

Scattering of harmonic plane P1 and SV waves by a circular lined tunnel in a poroelastic half-plane is investigated in this paper. An analytical approach is developed based on the complex variable function method and conformal mapping technique. In terms of the wave function expansions, the wave fields in the poroelastic medium and the liner are obtained for the displacements, effective stresses and fluid stress. Conformal mappings are introduced to transform the physical planes into two rings in the image plane for the medium and the liner,
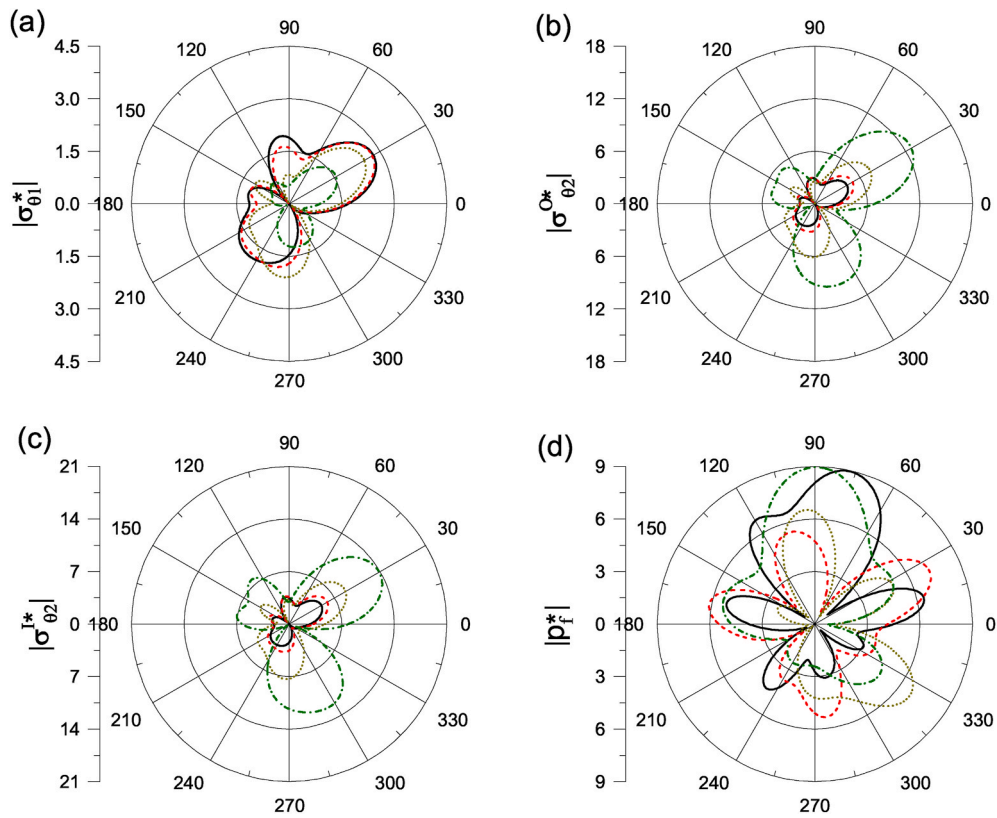
Fig. 12. Distribution of DSCFs and fluid stress by obliquely incident SV wave along the cavity wall with different porosity. (Solid line, $n = 0.05$; dash line, $n = 0.1$; dot line, $n = 0.2$; dash dot line, $n = 0.3$).

respectively. The boundary value problem is formulated by the boundary conditions and the continuity of the medium-liner interface as an infinite linear algebraic system. The convergence of the proposed method should be implemented by truncating the series number. The following conclusions can be drawn by a parametric study of the incident SV waves:

(1) The embedment depth of the tunnel has a significant influence on the displacements of the half surface. The shielding effect on the half surface by the tunnel is obvious to the incident SV waves.

(2) For the shallow tunnel, the effect of the embedment depth ratio on the DSCFs of the medium-liner interface and the liner and the fluid stress in the medium is great. When the embedment depth is big, the scattered waves contribute little to the displacements and the DSCFs of the liner.

(3) For a small porosity of the medium, its effect on the displacements of the half surface is weak. When the porosity is close to the critical value n_{cr}, the porosity contributes greatly to the response of the medium-liner system.

Author agreement

All authors have seen and approved the final version of the manuscript being submitted. We warrant that the article is the authors'

original work, hasn't received prior publication, and isn't under consideration for publication elsewhere.

Author statement

Qijian Liu: Conceptualization, Methodology, Supervision, Formal analysis, Writing- Original draft preparation, Writing-review & editing.

Cheng Yue: Software, Formal analysis, Validation, Writing- Original draft preparation.

Mingjuan Zhao: Software, Methodology.

Declaration of competing interest

The authors declare that they have no known competing financial interests or personal relationships that could have appeared to influence the work reported in this paper.

Appendix A

$$E_{1,1n} = \delta_f H_n^{(1)}\left(k_f |w_1 + ih|\right)\left(\frac{w_1 + ih}{|w_1 + ih|}\right)^n - \mu_1 k_f^2 H_{n-2}^{(1)}\left(k_f |w_1 + ih|\right)\left(\frac{w_1 + ih}{|w_1 + ih|}\right)^{n-2} \tag{A.1}$$

$$E_{1,2n} = \delta_s H_n^{(1)}\left(k_s |w_1 + ih|\right)\left(\frac{w_1 + ih}{|w_1 + ih|}\right)^n - \mu_1 k_s^2 H_{n-2}^{(1)}\left(k_s |w_1 + ih|\right)\left(\frac{w_1 + ih}{|w_1 + ih|}\right)^{n-2} \tag{A.2}$$

$$E_{1,3n} = -\mathrm{i}\mu_1 k_t^2 H_{n-2}^{(1)}(k_t|w_1 + \mathrm{i}h|)\left(\frac{w_1 + \mathrm{i}h}{|w_1 + \mathrm{i}h|}\right)^{n-2} \tag{A.3}$$

$$E_{1,4n} = \delta_f H_n^{(1)}\left(k_f|\overline{w_1} + \mathrm{i}h|\right)\left(\frac{\overline{w_1} + \mathrm{i}h}{|\overline{w_1} + \mathrm{i}h|}\right)^n - \mu_1 k_f^2 H_{n+2}^{(1)}\left(k_f|\overline{w_1} + \mathrm{i}h|\right)\left(\frac{\overline{w_1} + \mathrm{i}h}{|\overline{w_1} + \mathrm{i}h|}\right)^{n+2} \tag{A.4}$$

$$E_{1,5n} = \delta_s H_n^{(1)}(k_s|\overline{w_1} + \mathrm{i}h|)\left(\frac{\overline{w_1} + \mathrm{i}h}{|\overline{w_1} + \mathrm{i}h|}\right)^n - \mu_1 k_s^2 H_{n+2}^{(1)}(k_s|\overline{w_1} + \mathrm{i}h|)\left(\frac{\overline{w_1} + \mathrm{i}h}{|\overline{w_1} + \mathrm{i}h|}\right)^{n+2} \tag{A.5}$$

$$E_{1,6n} = -\mathrm{i}\mu_1 k_t^2 H_{n+2}^{(1)}(k_t|\overline{w_1} + \mathrm{i}h|)\left(\frac{\overline{w_1} + \mathrm{i}h}{|\overline{w_1} + \mathrm{i}h|}\right)^{n+2} \tag{A.6}$$

$$E_{1,7n} = 0 \tag{A.7}$$

$$E_{1,8n} = 0 \tag{A.8}$$

$$E_{1,9n} = 0 \tag{A.9}$$

$$E_{1,10n} = 0 \tag{A.10}$$

$$R_1 = 0 \tag{A.11}$$

$$E_{2,1n} = \delta_f H_n^{(1)}\left(k_f|w_1 + \mathrm{i}h|\right)\left(\frac{w_1 + \mathrm{i}h}{|w_1 + \mathrm{i}h|}\right)^n - \mu_1 k_f^2 H_{n+2}^{(1)}\left(k_f|w_1 + \mathrm{i}h|\right)\left(\frac{w_1 + \mathrm{i}h}{|w_1 + \mathrm{i}h|}\right)^{n+2} \tag{A.12}$$

$$E_{2,2n} = \delta_s H_n^{(1)}(k_s|w_1 + \mathrm{i}h|)\left(\frac{w_1 + \mathrm{i}h}{|w_1 + \mathrm{i}h|}\right)^n - \mu_1 k_s^2 H_{n+2}^{(1)}(k_s|w_1 + \mathrm{i}h|)\left(\frac{w_1 + \mathrm{i}h}{|w_1 + \mathrm{i}h|}\right)^{n+2} \tag{A.13}$$

$$E_{2,3n} = \mathrm{i}\mu_1 k_t^2 H_{n+2}^{(1)}(k_t|w_1 + \mathrm{i}h|)\left(\frac{w_1 + \mathrm{i}h}{|w_1 + \mathrm{i}h|}\right)^{n+2} \tag{A.14}$$

$$E_{2,4n} = \delta_f H_n^{(1)}\left(k_f|\overline{w_1} + \mathrm{i}h|\right)\left(\frac{\overline{w_1} + \mathrm{i}h}{|\overline{w_1} + \mathrm{i}h|}\right)^n - \mu_1 k_f^2 H_{n-2}^{(1)}\left(k_f|\overline{w_1} + \mathrm{i}h|\right)\left(\frac{\overline{w_1} + \mathrm{i}h}{|\overline{w_1} + \mathrm{i}h|}\right)^{n-2} \tag{A.15}$$

$$E_{2,5n} = \delta_s H_n^{(1)}(k_s|\overline{w_1} + \mathrm{i}h|)\left(\frac{\overline{w_1} + \mathrm{i}h}{|\overline{w_1} + \mathrm{i}h|}\right)^n - \mu_1 k_s^2 H_{n-2}^{(1)}(k_s|\overline{w_1} + \mathrm{i}h|)\left(\frac{\overline{w_1} + \mathrm{i}h}{|\overline{w_1} + \mathrm{i}h|}\right)^{n-2} \tag{A.16}$$

$$E_{2,6n} = \mathrm{i}\mu_1 k_t^2 H_{n-2}^{(1)}(k_t|\overline{w_1} + \mathrm{i}h|)\left(\frac{\overline{w_1} + \mathrm{i}h}{|\overline{w_1} + \mathrm{i}h|}\right)^{n-2} \tag{A.17}$$

$$E_{2,7n} = 0 \tag{A.18}$$

$$E_{2,8n} = 0 \tag{A.19}$$

$$E_{2,9n} = 0 \tag{A.20}$$

$$E_{2,10n} = 0 \tag{A.21}$$

$$R_2 = 0 \tag{A.22}$$

$$E_{3,1n} = -\alpha_f k_f^2 H_n^{(1)}\left(k_f|w_1 + \mathrm{i}h|\right)\left(\frac{w_1 + \mathrm{i}h}{|w_1 + \mathrm{i}h|}\right)^n \tag{A.23}$$

$$E_{3,2n} = -\alpha_s k_s^2 H_n^{(1)}(k_s|w_1 + \mathrm{i}h|)\left(\frac{w_1 + \mathrm{i}h}{|w_1 + \mathrm{i}h|}\right)^n \tag{A.24}$$

$$E_{3,3n} = 0 \tag{A.25}$$

$$E_{3,4n} = -\alpha_f k_f^2 H_n^{(1)}\left(k_f|\overline{w_1} + \mathrm{i}h|\right)\left(\frac{\overline{w_1} + \mathrm{i}h}{|\overline{w_1} + \mathrm{i}h|}\right)^n \tag{A.26}$$

$$E_{3,5n} = -\alpha_s k_s^2 H_n^{(1)}(k_s|\overline{w_1} + \mathrm{i}h|)\left(\frac{\overline{w_1} + \mathrm{i}h}{|\overline{w_1} + \mathrm{i}h|}\right)^n \tag{A.27}$$

$$E_{3,6n} = 0 \tag{A.28}$$

$$E_{3,7n} = 0 \tag{A.29}$$

$$E_{3,8n} = 0 \tag{A.30}$$

$$E_{3,9n} = 0 \tag{A.31}$$

$$E_{3,10n} = 0 \tag{A.32}$$

$$R_3 = 0 \tag{A.33}$$

$$E_{4,1n} = 0 \tag{A.34}$$

$$E_{4,2n} = 0 \tag{A.35}$$

$$E_{4,3n} = 0 \tag{A.36}$$

$$E_{4,4n} = 0 \tag{A.37}$$

$$E_{4,5n} = 0 \tag{A.38}$$

$$E_{4,6n} = 0 \tag{A.39}$$

$$E_{4,7n} = -(\lambda_2 + \mu_2) k_{L2}^2 H_n^{(1)}(k_{L2}|w_2 + ih|) \left(\frac{w_2 + ih}{|w_2 + ih|} \right)^n + \mu_2 k_{L2}^2 \frac{R_2^2 \overline{\zeta}^2}{R_1^2 \alpha^2} \frac{\overline{w_2'}}{w_2} H_{n+2}^{(1)}(k_{L2}|w_2 + ih|) \left(\frac{w_2 + ih}{|w_2 + ih|} \right)^{n+2} \tag{A.40}$$

$$E_{4,8n} = -(\lambda_2 + \mu_2) k_{L2}^2 H_n^{(2)}(k_{L2}|w_2 + ih|) \left(\frac{w_2 + ih}{|w_2 + ih|} \right)^n + \mu_2 k_{L2}^2 \frac{R_2^2 \overline{\zeta}^2}{R_1^2 \alpha^2} \frac{\overline{w_2'}}{w_2} H_{n+2}^{(2)}(k_{L2}|w_2 + ih|) \left(\frac{w_2 + ih}{|w_2 + ih|} \right)^{n+2} \tag{A.41}$$

$$E_{4,9n} = -i\mu_2 k_{T2}^2 \frac{R_2^2 \overline{\zeta}^2}{R_1^2 \alpha^2} \frac{\overline{w_2'}}{w_2'} H_{n+2}^{(1)}(k_{T2}|w_2 + ih|) \left(\frac{w_2 + ih}{|w_2 + ih|} \right)^{n+2} \tag{A.42}$$

$$E_{4,10n} = -i\mu_2 k_{T2}^2 \frac{R_2^2 \overline{\zeta}^2}{R_1^2 \alpha^2} \frac{\overline{w_2'}}{w_2'} H_{n+2}^{(2)}(k_{T2}|w_2 + ih|) \left(\frac{w_2 + ih}{|w_2 + ih|} \right)^{n+2} \tag{A.43}$$

$$R_4 = 0 \tag{A.44}$$

$$E_{5,1n} = 0 \tag{A.45}$$

$$E_{5,2n} = 0 \tag{A.46}$$

$$E_{5,3n} = 0 \tag{A.47}$$

$$E_{5,4n} = 0 \tag{A.48}$$

$$E_{5,5n} = 0 \tag{A.49}$$

$$E_{5,6n} = 0 \tag{A.50}$$

$$E_{5,7n} = -(\lambda_2 + \mu_2) k_{L2}^2 H_n^{(1)}(k_{L2}|w_2 + ih|) \left(\frac{w_2 + ih}{|w_2 + ih|} \right)^n + \mu_2 k_{L2}^2 \frac{R_2^2 \zeta^2}{R_1^2 \alpha^2} \frac{w_2'}{\overline{w_2'}} H_{n-2}^{(1)}(k_{L2}|w_2 + ih|) \left(\frac{w_2 + ih}{|w_2 + ih|} \right)^{n-2} \tag{A.51}$$

$$E_{5,8n} = -(\lambda_2 + \mu_2) k_{L2}^2 H_n^{(2)}(k_{L2}|w_2 + ih|) \left(\frac{w_2 + ih}{|w_2 + ih|} \right)^n + \mu_2 k_{L2}^2 \frac{R_2^2 \zeta^2}{R_1^2 \alpha^2} \frac{w_2'}{\overline{w_2'}} H_{n-2}^{(2)}(k_{L2}|w_2 + ih|) \left(\frac{w_2 + ih}{|w_2 + ih|} \right)^{n-2} \tag{A.52}$$

$$E_{5,9n} = i\mu_2 k_{T2}^2 \frac{R_2^2 \zeta^2}{R_1^2 \alpha^2} \frac{w_2'}{\overline{w_2'}} H_{n-2}^{(1)}(k_{T2}|w_2 + ih|) \left(\frac{w_2 + ih}{|w_2 + ih|} \right)^{n-2} \tag{A.53}$$

$$E_{5,10n} = i\mu_2 k_{T2}^2 \frac{R_2^2 \zeta^2}{R_1^2 \alpha^2} \frac{w_2'}{\overline{w_2'}} H_{n-2}^{(2)}(k_{T2}|w_2 + ih||) \left(\frac{w_2 + ih}{|w_2 + ih|} \right)^{n-2} \tag{A.54}$$

$$R_5 = 0 \tag{A.55}$$

$$E_{6,1n} = -k_f \frac{\overline{\zeta_1}}{\alpha} \frac{\overline{w_1'}}{|w_1'|} H_{n+1}^{(1)}(k_f|w_1 + ih|) \left(\frac{w_1 + ih}{|w_1 + ih|} \right)^{n+1} \tag{A.56}$$

$$E_{6,2n} = -k_s \frac{\overline{\zeta_1}}{\alpha} \frac{\overline{w_1'}}{|w_1'|} H_{n+1}^{(1)}(k_s|w_1 + ih|) \left(\frac{w_1 + ih}{|w_1 + ih|} \right)^{n+1} \tag{A.57}$$

$$E_{6,3n} = ik_t \frac{\overline{\zeta_1}}{\alpha} \frac{\overline{w_1'}}{|w_1'|} H_{n+1}^{(1)}(k_t|w_1 + ih|) \left(\frac{w_1 + ih}{|w_1 + ih|} \right)^{n+1} \tag{A.58}$$

$$E_{6,4n} = k_f \frac{\overline{\zeta_1}}{\alpha} \frac{\overline{w_1'}}{|w_1'|} H_{n-1}^{(1)}(k_f|\overline{w_1} + ih|) \left(\frac{\overline{w_1} + ih}{|\overline{w_1} + ih|} \right)^{n-1} \tag{A.59}$$

$$E_{6,5n} = k_s \frac{\overline{\zeta_1}}{\alpha} \frac{\overline{w_1'}}{|w_1'|} H_{n-1}^{(1)}(k_s|\overline{w_1} + ih|) \left(\frac{\overline{w_1} + ih}{|\overline{w_1} + ih|}\right)^{n-1} \tag{A.60}$$

$$E_{6,6n} = -ik_t \frac{\overline{\zeta_1}}{\alpha} \frac{\overline{w_1'}}{|w_1'|} H_{n-1}^{(1)}(k_t|\overline{w_1} + ih|) \left(\frac{\overline{w_1} + ih}{|\overline{w_1} + ih|}\right)^{n-1} \tag{A.61}$$

$$E_{6,7n} = k_{L2} \frac{\overline{\zeta}}{\alpha} \frac{\overline{w_2'}}{|w_2'|} H_{n+1}^{(1)}(k_{L2}|w_2 + ih|) \left(\frac{w_2 + ih}{|w_2 + ih|}\right)^{n+1} \tag{A.62}$$

$$E_{6,8n} = k_{L2} \frac{\overline{\zeta}}{\alpha} \frac{\overline{w_2'}}{|w_2'|} H_{n+1}^{(2)}(k_{L2}|w_2 + ih|) \left(\frac{w_2 + ih}{|w_2 + ih|}\right)^{n+1} \tag{A.63}$$

$$E_{6,9n} = -ik_{T2} \frac{\overline{\zeta}}{\alpha} \frac{\overline{w_2'}}{|w_2'|} H_{n+1}^{(1)}(k_{T2}|w_2 + ih|) \left(\frac{w_2 + ih}{|w_2 + ih|}\right)^{n+1} \tag{A.64}$$

$$E_{6,10n} = -ik_{T2} \frac{\overline{\zeta}}{\alpha} \frac{\overline{w_2'}}{|w_2'|} H_{n+1}^{(2)}(k_{T2}|w_2 + ih|) \left(\frac{w_2 + ih}{|w_2 + ih|}\right)^{n+1} \tag{A.65}$$

$$R_6 = -2 \frac{\overline{\zeta_1}}{\alpha|w_1'|} \frac{\partial}{\partial \overline{\zeta_1}} \left(\varphi_f^i + \varphi_f^r + \varphi_s^i + \varphi_s^r - i(\psi^i + \psi^r)\right) \tag{A.66}$$

$$E_{7,1n} = k_f \frac{\zeta_1}{\alpha} \frac{w_1'}{|w_1'|} H_{n-1}^{(1)}(k_f|w_1 + ih|) \left(\frac{w_1 + ih}{|w_1 + ih|}\right)^{n-1} \tag{A.67}$$

$$E_{7,2n} = k_s \frac{\zeta_1}{\alpha} \frac{w_1'}{|w_1'|} H_{n-1}^{(1)}(k_s|w_1 + ih|) \left(\frac{w_1 + ih}{|w_1 + ih|}\right)^{n-1} \tag{A.68}$$

$$E_{7,3n} = ik_t \frac{\zeta_1}{\alpha} \frac{w_1'}{|w_1'|} H_{n-1}^{(1)}(k_t|w_1 + ih|) \left(\frac{w_1 + ih}{|w_1 + ih|}\right)^{n-1} \tag{A.69}$$

$$E_{7,4n} = -k_f \frac{\zeta_1}{\alpha} \frac{w_1'}{|w_1'|} H_{n+1}^{(1)}(k_f|\overline{w_1} + ih|) \left(\frac{\overline{w_1} + ih}{|\overline{w_1} + ih|}\right)^{n+1} \tag{A.70}$$

$$E_{7,5n} = -k_s \frac{\zeta_1}{\alpha} \frac{w_1'}{|w_1'|} H_{n+1}^{(1)}(k_s|\overline{w_1} + ih|) \left(\frac{\overline{w_1} + ih}{|\overline{w_1} + ih|}\right)^{n+1} \tag{A.71}$$

$$E_{7,6n} = -ik_t \frac{\zeta_1}{\alpha} \frac{w_1'}{|w_1'|} H_{n+1}^{(1)}(k_t|\overline{w_1} + ih|) \left(\frac{\overline{w_1} + ih}{|\overline{w_1} + ih|}\right)^{n+1} \tag{A.72}$$

$$E_{7,7n} = -k_{L2} \frac{\zeta}{\alpha} \frac{w_2'}{|w_2'|} H_{n-1}^{(1)}(k_{L2}|w_2 + ih|) \left(\frac{w_2 + ih}{|w_2 + ih|}\right)^{n-1} \tag{A.73}$$

$$E_{7,8n} = -k_{L2} \frac{\zeta}{\alpha} \frac{w_2'}{|w_2'|} H_{n-1}^{(2)}(k_{L2}|w_2 + ih|) \left(\frac{w_2 + ih}{|w_2 + ih|}\right)^{n-1} \tag{A.74}$$

$$E_{7,9n} = -ik_{T2} \frac{\zeta}{\alpha} \frac{w_2'}{|w_2'|} H_{n-1}^{(1)}(k_{T2}|w_2 + ih|) \left(\frac{w_2 + ih}{|w_2 + ih|}\right)^{n-1} \tag{A.75}$$

$$E_{7,10n} = -ik_{T2} \frac{\zeta}{\alpha} \frac{w_2'}{|w_2'|} H_{n-1}^{(2)}(k_{T2}|w_2 + ih|) \left(\frac{w_2 + ih}{|w_2 + ih|}\right)^{n-1} \tag{A.76}$$

$$R_7 = -2 \frac{\zeta_1}{\alpha|w_1'|} \frac{\partial}{\partial \zeta_1} \left(\varphi_f^i + \varphi_f^r + \varphi_s^i + \varphi_s^r + i(\psi^i + \psi^r)\right) \tag{A.77}$$

$$E_{8,1n} = \delta_f H_n^{(1)}(k_f|w_1 + ih|) \left(\frac{w_1 + ih}{|w_1 + ih|}\right)^n + \mu_1 k_f^2 \frac{\overline{\zeta_1^2}}{\alpha^2} \frac{\overline{w_1'}}{w_1'} H_{n+2}^{(1)}(k_f|w_1 + ih|) \left(\frac{w_1 + ih}{|w_1 + ih|}\right)^{n+2} \tag{A.78}$$

$$E_{8,2n} = \delta_s H_n^{(1)}(k_s|w_1 + ih|) \left(\frac{w_1 + ih}{|w_1 + ih|}\right)^n + \mu_1 k_s^2 \frac{\overline{\zeta_1^2}}{\alpha^2} \frac{\overline{w_1'}}{w_1'} H_{n+2}^{(1)}(k_s|w_1 + ih|) \left(\frac{w_1 + ih}{|w_1 + ih|}\right)^{n+2} \tag{A.79}$$

$$E_{8,3n} = -i\mu_1 k_t^2 \frac{\overline{\zeta_1^2}}{\alpha^2} \frac{\overline{w_1'}}{w_1'} H_{n+2}^{(1)}(k_t|w_1 + ih|) \left(\frac{w_1 + ih}{|w_1 + ih|}\right)^{n+2} \tag{A.80}$$

$$E_{8,4n} = \delta_f H_n^{(1)}(k_f|\overline{w_1} + ih|) \left(\frac{\overline{w_1} + ih}{|\overline{w_1} + ih|}\right)^n + \mu_1 k_f^2 \frac{\overline{\zeta_1^2}}{\alpha^2} \frac{\overline{w_1'}}{w_1'} H_{n-2}^{(1)}(k_f|\overline{w_1} + ih|) \left(\frac{\overline{w_1} + ih}{|\overline{w_1} + ih|}\right)^{n-2} \tag{A.81}$$

$$E_{8,5n} = \delta_s H_n^{(1)}(k_s|\overline{w_1}+ih|)\left(\frac{\overline{w_1}+ih}{|\overline{w_1}+ih|}\right)^n + \mu_1 k_s^2 \frac{\overline{\zeta_1^2}}{\alpha^2}\frac{\overline{w_1}}{w_1}H_{n-2}^{(1)}(k_s|\overline{w_1}+ih|)\left(\frac{\overline{w_1}+ih}{|\overline{w_1}+ih|}\right)^{n-2} \tag{A.82}$$

$$E_{8,6n} = -i\mu_1 k_t^2 \frac{\overline{\zeta_1^2}}{\alpha^2}\frac{\overline{w_1}}{w_1}H_{n-2}^{(1)}(k_t|\overline{w_1}+ih|)\left(\frac{\overline{w_1}+ih}{|\overline{w_1}+ih|}\right)^{n-2} \tag{A.83}$$

$$E_{8,7n} = (\lambda_2+\mu_2)k_{L2}^2 H_n^{(1)}(k_{L2}|w_2+ih|)\left(\frac{w_2+ih}{|w_2+ih|}\right)^n - \mu_2 k_{L2}^2 \frac{\overline{\zeta^2}}{\alpha^2}\frac{\overline{w_2}}{w_2}H_{n+2}^{(1)}(k_{L2}|w_2+ih|)\left(\frac{w_2+ih}{|w_2+ih|}\right)^{n+2} \tag{A.84}$$

$$E_{8,8n} = (\lambda_2+\mu_2)k_{L2}^2 H_n^{(2)}(k_{L2}|w_2+ih|)\left(\frac{w_2+ih}{|w_2+ih|}\right)^n - \mu_2 k_{L2}^2 \frac{\overline{\zeta^2}}{\alpha^2}\frac{\overline{w_2}}{w_2}H_{n+2}^{(2)}(k_{L2}|w_2+ih|)\left(\frac{w_2+ih}{|w_2+ih|}\right)^{n+2} \tag{A.85}$$

$$E_{8,9n} = i\mu_2 k_{T2}^2 \frac{\overline{\zeta^2}}{\alpha^2}\frac{\overline{w_2}}{w_2}H_{n+2}^{(1)}(k_{T2}|w_2+ih|)\left(\frac{w_2+ih}{|w_2+ih|}\right)^{n+2} \tag{A.86}$$

$$E_{8,10n} = i\mu_2 k_{T2}^2 \frac{\overline{\zeta^2}}{\alpha^2}\frac{\overline{w_2}}{w_2}H_{n+2}^{(2)}(k_{T2}|w_2+ih|)\left(\frac{w_2+ih}{|w_2+ih|}\right)^{n+2} \tag{A.87}$$

$$R_8 = -\delta_f\left(\varphi_f^i+\varphi_f^r\right) - \delta_s\left(\varphi_s^i+\varphi_s^r\right) - 4\mu_1 \frac{\overline{\zeta_1^2}}{\alpha^2}\frac{1}{\overline{w_1}}\frac{\partial}{\partial\overline{\zeta_1}}\left[\frac{1}{\overline{w_1}}\frac{\partial}{\partial\overline{\zeta_1}}\left(\varphi_f^i+\varphi_f^r+\varphi_s^i+\varphi_s^r - i(\psi^i+\psi^r)\right)\right] \tag{A.88}$$

$$E_{9,1n} = \delta_f H_n^{(1)}(k_f|w_1+ih|)\left(\frac{w_1+ih}{|w_1+ih|}\right)^n + \mu_1 k_f^2 \frac{\zeta_1^2}{\alpha^2}\frac{w_1}{\overline{w_1}}H_{n-2}^{(1)}(k_f|w_1+ih|)\left(\frac{w_1+ih}{|w_1+ih|}\right)^{n-2} \tag{A.89}$$

$$E_{9,2n} = \delta_s H_n^{(1)}(k_s|w_1+ih|)\left(\frac{w_1+ih}{|w_1+ih|}\right)^n + \mu_1 k_s^2 \frac{\zeta_1^2}{\alpha^2}\frac{w_1}{\overline{w_1}}H_{n-2}^{(1)}(k_s|w_1+ih|)\left(\frac{w_1+ih}{|w_1+ih|}\right)^{n-2} \tag{A.90}$$

$$E_{9,3n} = i\mu_1 k_t^2 \frac{\zeta_1^2}{\alpha^2}\frac{w_1}{\overline{w_1}}H_{n-2}^{(1)}(k_t|w_1+ih|)\left(\frac{w_1+ih}{|w_1+ih|}\right)^{n-2} \tag{A.91}$$

$$E_{9,4n} = \delta_f H_n^{(1)}(k_f|\overline{w_1}+ih|)\left(\frac{\overline{w_1}+ih}{|\overline{w_1}+ih|}\right)^n + \mu_1 k_f^2 \frac{\zeta_1^2}{\alpha^2}\frac{w_1}{\overline{w_1}}H_{n+2}^{(1)}(k_f|\overline{w_1}+ih|)\left(\frac{\overline{w_1}+ih}{|\overline{w_1}+ih|}\right)^{n+2} \tag{A.92}$$

$$E_{9,5n} = \delta_s H_n^{(1)}(k_s|\overline{w_1}+ih|)\left(\frac{\overline{w_1}+ih}{|\overline{w_1}+ih|}\right)^n + \mu_1 k_s^2 \frac{\zeta_1^2}{\alpha^2}\frac{w_1}{\overline{w_1}}H_{n+2}^{(1)}(k_s|\overline{w_1}+ih|)\left(\frac{\overline{w_1}+ih}{|\overline{w_1}+ih|}\right)^{n+2} \tag{A.93}$$

$$E_{9,6n} = i\mu_1 k_t^2 \frac{\zeta_1^2}{\alpha^2}\frac{w_1}{\overline{w_1}}H_{n+2}^{(1)}(k_t|\overline{w_1}+ih|)\left(\frac{\overline{w_1}+ih}{|\overline{w_1}+ih|}\right)^{n+2} \tag{A.94}$$

$$E_{9,7n} = (\lambda_2+\mu_2)k_{L2}^2 H_n^{(1)}(k_{L2}|w_2+ih|)\left(\frac{w_2+ih}{|w_2+ih|}\right)^n - \mu_2 k_{L2}^2 \frac{\zeta^2}{\alpha^2}\frac{w_2}{\overline{w_2}}H_{n-2}^{(1)}(k_{L2}|w_2+ih|)\left(\frac{w_2+ih}{|w_2+ih|}\right)^{n-2} \tag{A.95}$$

$$E_{9,8n} = (\lambda_2+\mu_2)k_{L2}^2 H_n^{(2)}(k_{L2}|w_2+ih|)\left(\frac{w_2+ih}{|w_2+ih|}\right)^n - \mu_2 k_{L2}^2 \frac{\zeta^2}{\alpha^2}\frac{w_2}{\overline{w_2}}H_{n-2}^{(2)}(k_{L2}|w_2+ih|)\left(\frac{w_2+ih}{|w_2+ih|}\right)^{n-2} \tag{A.96}$$

$$E_{9,9n} = -i\mu_2 k_{T2}^2 \frac{\zeta^2}{\alpha^2}\frac{w_2}{\overline{w_2}}H_{n-2}^{(1)}(k_{T2}|w_2+ih|)\left(\frac{w_2+ih}{|w_2+ih|}\right)^{n-2} \tag{A.97}$$

$$E_{9,10n} = -i\mu_2 k_{T2}^2 \frac{\zeta^2}{\alpha^2}\frac{w_2}{\overline{w_2}}H_{n-2}^{(2)}(k_{T2}|w_2+ih|)\left(\frac{w_2+ih}{|w_2+ih|}\right)^{n-2} \tag{A.98}$$

$$R_9 = -\delta_f\left(\varphi_f^i+\varphi_f^r\right) - \delta_s\left(\varphi_s^i+\varphi_s^r\right) - 4\mu_1 \frac{\zeta_1^2}{\alpha^2}\frac{1}{\overline{w_1}}\frac{\partial}{\partial\zeta_1}\left[\frac{1}{\overline{w_1}}\frac{\partial}{\partial\zeta_1}\left(\varphi_f^i+\varphi_f^r+\varphi_s^i+\varphi_s^r + i(\psi^i+\psi^r)\right)\right] \tag{A.99}$$

$$E_{10,1n}^1 = -\alpha_f k_f^2 H_n^{(1)}(k_f|w_1+ih|)\left(\frac{w_1+ih}{|w_1+ih|}\right)^n \tag{A.100}$$

$$E_{10,2n}^1 = -\alpha_s k_s^2 H_n^{(1)}(k_s|w_1+ih|)\left(\frac{w_1+ih}{|w_1+ih|}\right)^n \tag{A.101}$$

$$E_{10,3n}^1 = 0 \tag{A.102}$$

$$E_{10,4n}^1 = -\alpha_f k_f^2 H_n^{(1)}(k_f|\overline{w_1}+ih|)\left(\frac{\overline{w_1}+ih}{|\overline{w_1}+ih|}\right)^n \tag{A.103}$$

$$E^1_{10,5n} = -\alpha_s k_s^2 H_n^{(1)}(k_s|\overline{w_1}+ih|)\left(\frac{\overline{w_1}+ih}{|\overline{w_1}+ih|}\right)^n \tag{A.104}$$

$$E^1_{10,6n} = 0 \tag{A.105}$$

$$E^1_{10,7n} = 0 \tag{A.106}$$

$$E^1_{10,8n} = 0 \tag{A.107}$$

$$E^1_{10,9n} = 0 \tag{A.108}$$

$$E^1_{10,10n} = 0 \tag{A.109}$$

$$R^1_{10} = \alpha_f k_f^2\left(\varphi_f^i+\varphi_f^r\right) + \alpha_s k_s^2\left(\varphi_s^i+\varphi_s^r\right) \tag{A.110}$$

$$E^2_{10,1n} = \eta_f k_f \frac{\zeta}{\alpha}\frac{w_1'}{|w_1'|}H_{n-1}^{(1)}\left(k_f|w_1+ih|\right)\left(\frac{w_1+ih}{|w_1+ih|}\right)^{n-1} - \eta_f k_f \frac{\overline{\zeta}}{\alpha}\frac{\overline{w_1'}}{|w_1'|}H_{n+1}^{(1)}\left(k_f|w_1+ih|\right)\left(\frac{w_1+ih}{|w_1+ih|}\right)^{n+1} \tag{A.111}$$

$$E^2_{10,2n} = \eta_s k_s \frac{\zeta}{\alpha}\frac{w_1'}{|w_1'|}H_{n-1}^{(1)}\left(k_s|w_1+ih|\right)\left(\frac{w_1+ih}{|w_1+ih|}\right)^{n-1} - \eta_s k_s \frac{\overline{\zeta}}{\alpha}\frac{\overline{w_1'}}{|w_1'|}H_{n+1}^{(1)}\left(k_s|w_1+ih|\right)\left(\frac{w_1+ih}{|w_1+ih|}\right)^{n+1} \tag{A.112}$$

$$E^2_{10,3n} = i\eta_t k_t \frac{\zeta}{\alpha}\frac{w_1'}{|w_1'|}H_{n-1}^{(1)}\left(k_t|w_1+ih|\right)\left(\frac{w_1+ih}{|w_1+ih|}\right)^{n-1} + i\eta_t k_t \frac{\overline{\zeta}}{\alpha}\frac{\overline{w_1'}}{|w_1'|}H_{n+1}^{(1)}\left(k_t|w_1+ih|\right)\left(\frac{w_1+ih}{|w_1+ih|}\right)^{n+1} \tag{A.113}$$

$$E^2_{10,4n} = -\eta_f k_f \frac{\zeta}{\alpha}\frac{w_1'}{|w_1'|}H_{n+1}^{(1)}\left(k_f|\overline{w_1}+ih|\right)\left(\frac{\overline{w_1}+ih}{|\overline{w_1}+ih|}\right)^{n+1} + \eta_f k_f \frac{\overline{\zeta}}{\alpha}\frac{\overline{w_1'}}{|w_1'|}H_{n-1}^{(1)}\left(k_f|\overline{w_1}+ih|\right)\left(\frac{\overline{w_1}+ih}{|\overline{w_1}+ih|}\right)^{n-1} \tag{A.114}$$

$$E^2_{10,5n} = -\eta_s k_s \frac{\zeta}{\alpha}\frac{w_1'}{|w_1'|}H_{n+1}^{(1)}\left(k_s|\overline{w_1}+ih|\right)\left(\frac{\overline{w_1}+ih}{|\overline{w_1}+ih|}\right)^{n+1} + \eta_s k_s \frac{\overline{\zeta}}{\alpha}\frac{\overline{w_1'}}{|w_1'|}H_{n-1}^{(1)}\left(k_s|\overline{w_1}+ih|\right)\left(\frac{\overline{w_1}+ih}{|\overline{w_1}+ih|}\right)^{n-1} \tag{A.115}$$

$$E^2_{10,6n} = -i\eta_t k_t \frac{\zeta}{\alpha}\frac{w_1'}{|w_1'|}H_{n+1}^{(1)}\left(k_t|\overline{w_1}+ih|\right)\left(\frac{\overline{w_1}+ih}{|\overline{w_1}+ih|}\right)^{n+1} - i\eta_t k_t \frac{\overline{\zeta}}{\alpha}\frac{\overline{w_1'}}{|w_1'|}H_{n-1}^{(1)}\left(k_t|\overline{w_1}+ih|\right)\left(\frac{\overline{w_1}+ih}{|\overline{w_1}+ih|}\right)^{n-1} \tag{A.116}$$

$$E^2_{7,10n} = 0 \tag{A.117}$$

$$E^2_{8,10n} = 0 \tag{A.118}$$

$$E^2_{9,10n} = 0 \tag{A.119}$$

$$E^2_{10,10n} = 0 \tag{A.120}$$

$$R^2_{10} = -2\frac{\zeta}{\alpha|w_1'|}\frac{\partial}{\partial\zeta}\left[\eta_f\left(\varphi_f^i+\varphi_f^r\right) + \eta_s\left(\varphi_s^i+\varphi_s^r\right) + i\eta_t\left(\psi^i+\psi^r\right)\right] - 2\frac{\overline{\zeta}}{\alpha|w_1'|}\frac{\partial}{\partial\overline{\zeta}}\left[\eta_f\left(\varphi_f^i+\varphi_f^r\right) + \eta_s\left(\varphi_s^i+\varphi_s^r\right) - i\eta_t\left(\psi^i+\psi^r\right)\right] \tag{A.121}$$

References

[1] Hashash YMA, Hook JJ, Schmidt B, Yao JIC. Seismic design and analysis of underground structures. Tunn Undergr Space Technol 2001;16:247–93.

[2] Moore ID, Guan F. Three-dimensional dynamic response of lined tunnels due to incident seismic waves. Earthq Eng Struct Dynam 1996;25:357–69.

[3] Pao HY, Mow CC. The diffraction of elastic waves and dynamic stress concentrations. New York: Crane-Russak; 1973.

[4] Zimmerman C, Stern M. Boundary element solution of 3-D wave scatter problems in a poroelastic medium. Eng Anal Bound Elem 1993;12:223–40.

[5] de Barros FCP, Luco JE. Diffraction of obliquely incident waves by a cylindrical cavity embedded in a layered viscoelastic half-space. Soil Dynam Earthq Eng 1993; 12:159–71.

[6] Luco JE, de Barros FCP. Dynamic displacements and stresses in the vicinity of a cylindrical cavity embedded in a half-space. Earthq Eng Struct Dynam 1994;23: 321–40.

[7] Niu Y, Dravinski M. Direct 3D BEM for scattering of elastic waves in a homogeneous anisotropic half-space. Wave Motion 2003;38:165–75.

[8] Liang J, You H, Lee VW. Scattering of SV waves by a canyon in a fluid-saturated, poroelastic layered half-space, modeled using the indirect boundary element method. Soil Dynam Earthq Eng 2006;26:611–25.

[9] Liang J, Liu Z. Diffraction of plane SV waves by a cavity in poroelastic half-space. Earthq Eng Eng Vib 2009;8(1):29–46.

[10] Yu CW, Dravinski M. Scattering of plane harmonic P, SV and Rayleigh waves by a completely embedded corrugated elastic inclusion. Wave Motion 2010;47:156–67.

[11] Dravinski M, Yu CW. Peak surface motion due to scattering of plane harmonic P, SV, or Rayleigh waves by a rough cavity embedded in an elastic half-space. J Seismol 2011;15:131–45.

[12] Alielahi H, Kamalian M, Adampira M. A BEM investigation on the influence of underground cavities on the seismic response of canyons. Acta Geotechnica 2016; 11:391–413.

[13] Liu Z, Ju X, Wu C, Liang J. Scattering of plane P1 waves and dynamic stress concentration by a lined tunnel in a fluid-saturated poroelastic half-space. Tunn Undergr Space Technol 2017;67:71–84.

[14] Huang L, Liu Z, Ju X, Wu C, Liang J. The scattering of plane P, SV waves by twin lining tunnels with imperfect interfaces embedded in an elastic half-space. Tunn Undergr Space Technol 2019;85:319–30.

[15] Panji M, Habibivand M. Seismic analysis of semi-sine shaped alluvial hills above subsurface circular cavity. Earthq Eng Eng Vib 2020;19:903–17.

[16] Gregory RD. An expansion theorem applicable to problems of wave propagation in an elastic half-space containing a cavity. Proc Camb Phil Soc 1967;63:1341–67.

[17] Gregory RD. The propagation of waves in an elastic half-space containing a cylindrical cavity. Proc Camb Phil Soc 1970;67:689–710.

[18] Martin PA. Scattering by defects in an exponentially graded layer and misuse of the method of images. Int J Solid Struct 2011;48:2164–6.

[19] Martin PA. Scattering by a cavity in an exponentially graded half-space. J Appl Mech 2009;76. 031009–1-031009-4.

[20] Lin CH, Lee VW, Todorovska M, Trifunac MD. Zero-stress, cylindrical wave functions around a circular underground tunnel in a flat, elastic half-space: incident P-waves. Soil Dynam Earthq Eng 2010;30(10):879–94.

[21] Lee VW, Cao H. Diffraction of SV waves by circular cylindrical canyons of various depths. J Eng Mech, ASCE 1989;115(9). 2035-56.

[22] Lee VW, Karl J. Diffraction of SV waves by underground, circular, cylindrical cavities. Soil Dynam Earthq Eng 1992;11:445–56.

[23] Lee VW, Trifunac MD. Response of tunnels to incident SH-waves. J Eng Mech, ASCE 1979;105:643–59.

[24] Davis CA, Lee VW, Bardet JP. Transverse response of underground cavities and pipes to incident SV waves. Earthq Eng Struct Dynam 2001;30:383–410.

[25] Liang J, Zhang H, Lee VW. A series solution for surface motion amplification due to underground twin tunnels: incident SV waves. Earthq Eng Eng Vib 2003;2(2): 289–98.

[26] Li W, Zhao C. Scattering of plane SV waves by cylindrical canyons in saturated porous medium. Soil Dynam Earthq Eng 2005;25:981–95.

[27] Liang J, Ba Z, Lee VW. Diffraction of plane SV waves by an underground circular cavity in a saturated poroelastic half-space. ISET J Earthq Technol 2007;44(2): 341–75.

[28] Smerzini C, Avilés J, Paolucci R, Sánchez-Sesma FJ. Effect of underground cavities on surface earthquake ground motion under SH wave propagation. Earthq Eng Struct Dynam 2009;38:1441–60.

[29] Jiang L, Zhou X, Wang J. Scattering of a plane wave by a lined cylindrical cavity in a poroelastic half-plane. Comput Geotech 2009;36:773–86.

[30] Liang J, Ba Z, Lee VW. Diffraction of plane SV waves by a shallow circular-arc canyon in a saturated poroelastic half-space. Soil Dynam Earthq Eng 2006;26: 582–610.

[31] Wang J, Lu J, Zhou X. Complex variable function method for the scattering of plane waves by an arbitrary hole in a porous medium. Eur J Mech Solid 2009;28:582–90.

[32] Abramowitz M, Stegun IA. Handbook of mathematical functions, with formulas, graphs, and mathematical tables. In: National Bureau of Standards: Washington, DC; 1964.

[33] Watson GN. A treatise on the theory of Bessel function. Cambridge: University Press; 1962.

[34] Lamb H. On the propagation of tremors over the surface of an elastic solid. Philos Trans Roy Soc London A 1904;203:1–42.

[35] Lee VW, Liu W. Two-dimensional scattering and diffraction of P- and SV-waves around a semi-circular canyon in an elastic half-space: an analytic solution via a stress-free wave function. Soil Dynam Earthq Eng 2014;63:110–9.

[36] Zhang N, Zhang Y, Gao Y, Pak RYS, Yang J. Site amplification effects of a radially multi-layered semi-cylindrical canyon on seismic response of an earth and rockfill dam. Soil Dynam Earthq Eng 2019;116:145–63.

[37] Li W, Zhu S, Lee VW, Shi P, Zhao Z. Scattering of plane SV-waves by a circular lined tunnel in an undersea saturated half-space. Soil Dynam Earthq Eng 2022;153: 107064.

[38] Liu D, Gai B, Tao G. Applications of the method of complex functions to dynamic stress concentration. Wave Motion 1982;4:293–304.

[39] Liu Q, Zhao M, Wang L. Scattering of plane P, SV or Rayleigh waves by a shallow lined tunnel in an elastic half space. Soil Dynam Earthq Eng 2013;49:52–63.

[40] Biot MA. Theory of propagation of elastic waves in a fluid-saturated porous solid: I. Low frequency range. J Acoust Soc Am 1956;28:168–78.

[41] Deresiewicz H. The effect of boundaries on wave propagation in a liquid-filled porous solid: I. Reflection of plane waves at a free plan boundary(non-dissipative case). Bull Seismol Soc Am 1960;50(4):599–607.

[42] Berryman JG. Confirmation of Biot's theory. Appl Phys Lett 1980;34(4):382–4.

[43] Hasheminejad SM, Avazmohammadi R. Harmonic wave diffraction by two circular cavities in a poroelastic formation. Soil Dynam Earthq Eng 2007;27:29–41.

[44] Biot MA, Willis DG. The elastic coefficients of the theory of consolidation. J Appl Mech 1957;24:594–601.

[45] Lin C, Lee VW, Trifunac MD. The reflection of plane waves in a poroelastic half-space saturated with inviscid fluid. Soil Dynam Earthq Eng 2005;25:205–23.

[46] Achenbach JD. Wave propagation in elastic solids. North-Holland,Amsterdam. 1973.

[47] Graff KF. Wave motion in elastic solids. Columbus, OH: Ohio State University Press; 1975.

[48] Verruijt A. Deformations of an elastic half plane with a circular cavity. Int J Solid Struct 1998;35:2795–804.

[49] Biot MA. Theory of elasticity and consolidation for a porous anisotropic solid. J Appl Phys 1955;26:182–5.